Throughput Optimization for NOMA Energy Harvesting Cognitive Radio with Multi-UAV-Assisted Relaying under Security Constraints

Viet-Hung Dang, Le-Mai-Duyen Nguyen, Van Nhan Vo, Hung Tran, Tu Dac Ho, *Member, IEEE* Chakchai So-In, *Senior Member, IEEE,* Surasak Sanguanpong, *Member, IEEE*

***Abstract*—This paper investigates the throughput of a non-orthogonal multiple access (NOMA)-based cognitive radio (CR) system with multiple unmanned aerial vehicle (UAV)-assisted relays under system performance and security constraints. We propose a communication protocol that includes an energy harvesting (EH) phase and multiple communication phases. In the EH phase, the multiple UAV relays (URs) harvest energy from a power beacon. In the first communication phase, a secondary transmitter (ST) uses the collected energy to send confidential signals to the first UR using NOMA. Simultaneously, a ground base station communicates with a primary receiver (PR) under interference from the ST. In the subsequent communication phases, the next URs apply the decode-and-forward technique to transmit the signals. In the last communication phase, the Internet of Things destinations (IDs) receive their signals in the presence of an eavesdropper (EAV). Accordingly, the outage probability of the primary network, the throughput of the secondary network, and the leakage probability at the EAV are analyzed. On this basis, we propose a hybrid search method combining particle swarm optimization (PSO) and continuous genetic algorithm (CGA) to optimize the UR configurations and the NOMA power allocation to maximize the throughput of the secondary network under performance and security constraints.**

***Index Terms*—Cognitive Radio (CR), Non-Orthogonal Multiple Access (NOMA), Unmanned Aerial Vehicle (UAV), Hybrid CGA-PSO, Security Constraints**

V.-H. Dang and V. N. Vo are with the Faculty of Information Technology, Duy Tan University, Da Nang 550000, Vietnam, and the Institute of Research and Development, Duy Tan University, Da Nang 550000, Vietnam (e-mail: dangviethung@duytan.edu.vn and vonhanvan@dtu.edu.vn).

L.-M.-D. Nguyen is with the Faculty of Electrical-Electronic Engineering, Duy Tan University, Da Nang 550000, Vietnam, and the Institute of Research and Development, Duy Tan University, Da Nang 550000, Vietnam (e-mail: nguyenlmaiduyen@duytan.edu.vn).

H. Tran is with the Faculty of Computer Science, Phenikaa University, Hanoi 12116, Vietnam (e-mail: hung.tran@phenikaa-uni.edu.vn).

T. D. Ho is with the Department of Electrical Engineering, Faculty of Engineering Science and Technology, UiT – The Arctic University of Norway (email: Tu.D.Ho@uit.no).

C. So-In is with the Applied Network Technology (ANT) Laboratory, College of Computing, Khon Kaen University, Thailand 40002, Thailand (e-mail: chakso@kku.ac.th).

S. Sanguanpong is with the Department of Computer Engineering, Faculty of Engineering, Kasetsart University, Bangkok 10900, Thailand (e-mail: surasak.s@ku.ac.th).

Corresponding author: Surasak Sanguanpong.

I. Introduction

Cognitive radio (CR) is widely regarded as a potential solution for addressing the issue of spectrum scarcity, which has been exacerbated by the massive growth of wireless data traffic in fifth generation (5G) communication systems and beyond [1]. More specifically, CR provides public access to underused spectral bands, allowing unlicensed (cognitive) users to exploit the licensed spectrum from an opportunistic standpoint and hence economically enhancing the overall spectral efficiency [2].

Furthermore, considering the requirements of 5G systems, especially spectral efficiency and massive-scale connectivity, non-orthogonal multiple access (NOMA) can be a complementary solution to the CR technique because it provides the capacity to boost connectivity when restricted radio resources are available [3]. In NOMA, the entire bandwidth may be used simultaneously by different users at different power levels [4]. For example, the authors of [5] investigated a relaying scheme in a NOMA-based CR (CR-NOMA) system with a primary transmitter (PT), a primary receiver (PR), a secondary transmitter (ST), a relay, and two secondary

receivers (SRs). Closed-form expressions for the outage probability were derived to evaluate the system performance of the two SRs over both Rayleigh fading and Nakagami-m fading channels. As an extension of this work, Z. Xiang *et al.* considered a CR-NOMA system with a PT, an ST, multiple PRs, and multiple SRs. The authors concluded that the combination of NOMA and CR can reduce the mutual interference among signals and that the system throughput for a massive number of users is better with NOMA than it is with orthogonal multiple access (OMA) [6]. However, these two works focused only on fixed power allocation, which cannot support optimization of the system performance. To solve this issue, this work investigates dynamic power allocation and finds the optimal values of the power allocation factors to improve the system performance.

Building on the previous efforts discussed above, [3] studied the outage and throughput performance of a CR-NOMA system. Specifically, the secondary network used NOMA and decode-and-forward (DF) relays to deliver information from a ground base station (GBS) to the SRs. The authors derived closed-form expressions for the outage probabilities and then obtained a closed-form expression for the optimal power allocation (OPA) factors at the GBS to maximize the throughput of the secondary network in the studied CR-NOMA system. They concluded that through optimization of the OPA factors, the system performance of the secondary network in CR-NOMA can be significantly improved compared to equal and random power allocation schemes. Nonetheless, the large-scale connectivity and obstruction by obstacles in CR networks cause a decrease in system throughput.

To address the above challenges, unmanned aerial vehicle (UAV)-assisted relaying is an effective means of improving the system performance [7], [8]. A UAV has an enhanced likelihood of line-of-sight (LoS) conditions because of its ability to adapt its pose to circumvent barriers [9]. For example, [8] investigated the achievable rates of a CR system with a UAV-assisted relay. To analyze the system performance, the authors derived an expression for the power level that maximizes both the primary and secondary rates. They concluded that UAV-assisted relaying may be used in conjunction with CR technology to increase both rates by exploiting the flexibility, independence, and other qualities of UAVs. However, a UAV's operation is dependent on battery power. Hence, a network aided by UAVs is an energy-constrained network.

In an energy-constrained network, radio frequency (RF) energy harvesting (EH) is an effective and environmentally friendly method for recharging batteries. Consequently, the concept of EH has attracted considerable attention as a viable strategy for overcoming the energy limits of UAV-assisted networks [10]–[13]. For example, [10] focused on a CR network in which a UAV was used as a relay, i.e., a UAV relay (UR), to support communication from an ST to an SR. Then, an optimization algorithm was proposed to achieve the optimal system performance for the UAV CR network. The numerical results showed that the proposed algorithm could achieve a fast coverage rate and optimize the UAV path. Notably, however, interference with the secondary network from the primary network was not considered in that work.

To address this shortcoming, [13] investigated the interference issue for a cooperative transmission mechanism in a CR network in which the primary and secondary networks shared a dedicated RF source with DF UAV selection. The numerical results of a simulation verified the mechanism's efficiency and the correctness of the calculation. However, the NOMA technique was not considered in that work. Hence, the authors of [11] addressed the case of CR-NOMA using an EH UAV relay. The UAV harvested energy from the RF signals from source nodes. The authors obtained closed-form expressions for the harvested energy and throughput and then optimized the power allocation to maximize the network throughput. They concluded that the EH technique can minimize power consumption and increase throughput.

However, UAVs also face security issues as a result of their radio broadcast features. Consequently, such issues have become a prominent research topic in recent years, with many scientists studying communication secrecy and privacy protection [13], [14]. In this context, secure physical-layer transmission has gained widespread acceptance as a viable solution for ensuring wireless transmission secrecy in the future [13], [14]. For example, [13] investigated a CR system in which an ST can sense a dedicated DF source of a PT in order to transmit signals to SRs with DF UAV selection and EH in a cognitive network under monitoring by an eaves-

dropper (EAV). The authors then derived closed-form expressions for the secrecy outage probability (SOP) and the probability of a nonzero secrecy capacity by using the function analysis method to evaluate the secrecy performance. The quantitative results indicated that the proposed system using physical-layer security technology can achieve improved system security. However, the authors assumed perfect channel state information (CSI) and successive interference cancellation (SIC), which is impossible to guarantee in a practical scenario. To overcome these drawbacks, this work considers large-scare connectivity, obstruction by obstacles, energy constraints, security problems, and imperfect CSI and SIC to develop an analysis that can generalize well to practical scenarios.

Based on the obtained closed-form expressions, many optimization methods have been proposed to find the best UAV positions or the best power allocation or EH time with the aim of maximizing throughput or security probabilities. However, there are no previous works that have collectively optimized all relevant parameters while simultaneously considering security constraints. Moreover, the existing heuristic optimization methods for cognitive systems are not good enough for our problem, which is a complex problem with a high-dimensional search space in which the number of UAVs and their positions can be varied. Certainly, an exhaustive brute-force search would not be applicable even with discretization of the continuous search space because the high dimensionality of the search space would lead to combinatorial explosion.

Moreover, calculus-based optimization methods such as gradient descent, the Newton–Raphson method, and the conjugate gradient method are suitable only for either convex or single-maximum objective functions. For our problem, suboptimal heuristic search methods are more suitable because they allow both uphill search and random search simultaneously using knowledge of multiple individual solution candidates. This can help the search escape from local maxima and increases the probability of finding the global maximum. There are several popular algorithms of this kind that have recently been applied to solve optimization problems, including simulated annealing (SA), genetic algorithms (GAs), and particle swarm optimization (PSO) [15]–[20]. Due to the demand for real-time response and better results, a few updated versions of these methods have also been developed by combining two of them, as in [21]–[24].

In these updated methods, a GA and PSO are usually the best candidates for combination because PSO has the advantage of quick convergence, while a GA can achieve efficient exploration [21], [22]. In [21], a hybrid algorithm combining PSO with a GA was presented in which every candidate in the population is forced to move twice with certain velocities. One move is toward the current global best candidate, and the other is toward the candidate's own historical best solution. These movements replace the GA phases of crossover and mutation. This method achieves better objective results than PSO because it allows more exploration in the search process by making candidates move not only toward the global best solution but also toward their own best versions. However, the exploration ability of this method is still insufficient; consequently, the search usually becomes trapped in a local maximum when dealing with a problem with multiple local maxima, such as ours.

Another hybrid GA-PSO method was proposed in [22], attempting to utilize the exploration ability of a GA by randomly dividing the whole population into two subpopulations at the beginning of every generation. Then, one subpopulation is evolved with the GA, while the other is evolved with PSO. This algorithm also yields improved objective values since the probability of escaping from local maxima is higher. Nevertheless, the trade-off between the run time and the final objective value remains significant.

To overcome the weaknesses of [21] (weak exploration) and [22] (strong exploration but a long run time), this work aims to develop another heuristic algorithm that inherits the strengths of both the GA and PSO approaches in a simpler and more clever way, mitigating the trade-off of run time for a higher final objective value.

As seen from the above summary, no existing work using multihop EH URs in a CR-NOMA network has studied system performance optimization for the secondary network under constraints on the outage probability of the primary network and the leakage probability at the EAV. More generally, no previous work has considered the high-dimensional optimization problem of optimizing all adjustable system parameters subject to constraints. The present work addresses this gap in the literature,

with the following primary contributions:

- We investigate a CR-NOMA system in which a GBS sends signals to a PR using OMA, while with the help of multiple EH URs, an ST transmits information to Internet of Things (IoT) destinations (IDs) using NOMA under monitoring by an EAV.
- We propose a communication protocol for the considered system and analyze the system and security performance of the primary and secondary networks.
- We propose a hybrid machine learning (ML) algorithm to solve the constrained optimization problem for resource allocation to determine the number and positions of the URs such that the PR can decode the signals from the GBS.

The rest of this paper is organized as follows. Section II introduces the system model and communication protocol. Section III presents the closed-form expressions for the performance analysis and the formulation of the optimization problem. In Section IV, we present the hybrid ML algorithm proposed to solve our optimization problem. Simulation results are presented and discussed in Section V, and conclusions are given in Section VI.

II. System Model and Communication Protocol

A. System model and channel assumptions

Let us consider a CR-NOMA system as shown in Fig. 1 for a scenario in which spectrum resources are limited and obstacles (e.g., high buildings and forests) cover large areas and block the LoS paths. In particular, the primary users (PUs) (the GBS and PR) license the spectrum by using the OMA principle because OMA is superior to NOMA from an energy perspective when applied in a one-to-one scheme [25]. Meanwhile, the secondary users (SUs) (the ST, URs, and IDs, i.e., ID_p and ID_q, where $1 \leq p, q \leq Q$) attempt to utilize the licensed spectrum by using the NOMA technique for their communication, provided that their transmit power does not interrupt the communication of the PUs. Here, NOMA is applied because it outperforms OMA in terms of throughput when applied in a one-to-many scheme. Because of the presence of obstacles, the ST cannot communicate directly with the IDs; therefore, UAV-assisted relays (i.e., the URs) are adopted to increase the transmission distance under the influence of obstacles [9], [11]. Based on the concept of green communications, an EH scheme is applied at the URs to save power and minimize carbon emissions by collecting energy from a power beacon (PB) [26]. Furthermore, due to the broadcast nature of the communication, an EAV near the IDs has the opportunity to steal confidential signals from the last UR; note, however, that the EAV has no link to any of the other URs because of their farther distances [13], [14].

Suppose that the GBS is equipped with V antennas, while the PR, PB, ST, IDs, and URs are each equipped with a single antenna [13], [26], [27]. For the GBS–PR, ST–PR, ST–UR_1, UR_1–PR, UR_n–UR_{n+1}, UR_N–D_p, UR_N–D_q, GBS–UR_N, GBS–D_p, GBS–D_p, UR_N–E, and GBS–E links, the channel gains are denoted by g_{G_vP}, g_{SP}, g_{SU_1}, $g_{U_nU_{n+1}}$, $g_{U_ND_p}$, $g_{U_ND_p}$, $g_{G_vU_N}$, $g_{G_vD_p}$, $g_{G_vD_q}$, g_{U_NE}, and g_{G_vE}, respectively, and the distances are denoted by d_{G_vP}, d_{SP}, d_{SU_1}, $d_{U_nU_{n+1}}$, $d_{U_ND_p}$, $d_{U_ND_p}$, $d_{G_vU_N}$, $d_{G_vD_p}$, $d_{G_vD_q}$, d_{U_NE}, and d_{G_vE}, respectively, where N is the number of URs, $n \in \{1, \ldots, N\}$, and $v \in \{1, \ldots, V\}$. This model scheme is a centralized implementation, in which there is a central controller, referred to as the CR network manager, established at the ST. The PT obtains information from the PR, while the ST gathers network information from the UR and IDs, and the last UR obtains information from the EAV. The central controller will receive the CSI from the PT and ST and then forward some appropriately quantized CSI to the ST and PT (and to the IDs and PR for decoding purposes) through a finite-rate feedback link [28], [29].

Here, all channel gains are independent and identically distributed (i.i.d.) and remain constant for the duration of one packet. In particular, for ground-to-ground communication, the channel gains are modeled as the gains of Rayleigh fading channels, i.e., random variables (RVs) distributed following an exponential distribution [30]. Thus, the probability density functions (PDFs) and cumulative distribution functions (CDFs) of the channel gains are formulated as follows:

$$f_{g_a}(x) = \frac{1}{\Omega_a} \exp\left(-\frac{x}{\Omega_a}\right), \tag{1}$$

$$F_{g_a}(x) = 1 - \exp\left(-\frac{x}{\Omega_a}\right), \tag{2}$$

where $a \in \{SP, G_vP, G_vD_p, G_vD_q, GE\}$ is an RV with a mean value of $\Omega_a = \mathbf{E}[a]$.

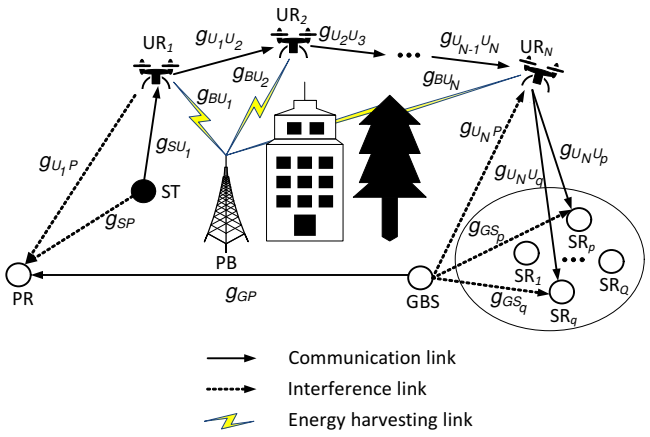

Fig. 1: A CR-NOMA IoT architecture.

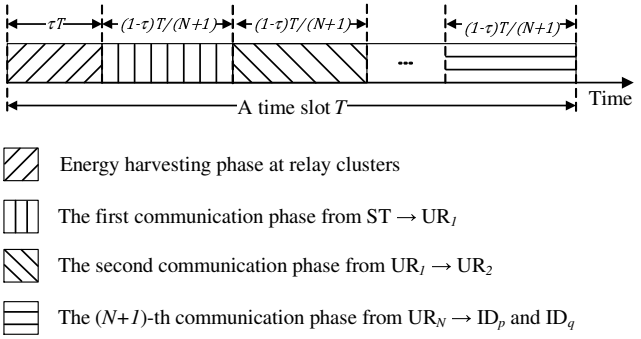

Fig. 2: The time switching (TS) transmission protocol.

For air-to-ground and ground-to-air communication, the path loss models are expressed as absolute values $\overline{L}_b = \beta_b d_b^{\eta_b}$, where $b \in \{SU_1, U_N D_p, U_N D_q, U_N E\}$. According to [31], a ground-to-air channel is more likely to be dominated by either LoS conditions or non-line-of-sight (NLoS) conditions depending on the environment (e.g., suburban, urban, or dense urban). Here, we assume that $\eta_b = 2$; thus, the quantity β_b is formulated as $\beta_b = 10^B$ [32], in which B is defined as

$$B = \frac{10\log_{10}\left(4\pi f/c\right)^2 + \omega_{NLoS}}{10} + \frac{\omega_{LoS} - \omega_{NLoS}}{10 + 10\varphi\exp\left[-\psi\left(\frac{180}{\pi}\theta - \varphi\right)\right]}, \quad (3)$$

where θ is the elevation angle of the UR with respect to either the GBS, ST, or IDs; φ and ψ are constants that depend on the environment [33]; and ω_{LoS} and ω_{NLoS} are environment- and frequency-dependent parameters that represent the excess path losses of LoS and NLoS links, respectively [33]. For air-to-air communication, the path loss can be expressed as $\overline{L}_{U_n U_{n+1}} = \beta_{U_n U_{n+1}} d_{U_n U_{n+1}}^{\eta_{U_n U_{n+1}}}$, where $\beta_{U_n U_{n+1}} = \left(\frac{4\pi f}{c}\right)^2$ [32].

Furthermore, the ground-to-air, air-to-ground, and air-to-air channel gains are consistent with a Nakagami-m distributed fading environment with fading severity parameter m [9], i.e., RVs following a Gamma distribution. Thus, the PDF and CDF of the channel gain g_α are formulated as follows:

$$f_{g_\alpha}(x) = \left(\frac{m_\alpha}{\Omega_\alpha}\right)^{m_\alpha} \frac{x^{m_\alpha - 1}}{\Gamma(m_\alpha)} \exp\left(-\frac{m_\alpha x}{\Omega_\alpha}\right), \quad (4)$$

$$F_{g_\alpha}(x) = 1 - \sum_{j=0}^{m_\alpha - 1} \left(\frac{m_\alpha x}{\Omega_\alpha}\right)^j \frac{1}{j!} \exp\left(-\frac{m_\alpha x}{\Omega_\alpha}\right), \quad (5)$$

where $\alpha \in \{b, U_n U_{n+1}\}$, g_α is an RV with a mean value of $\Omega_\alpha = \mathbf{E}\left[|g_\alpha|^2\right]$, and $\Gamma(\cdot)$ is the Gamma function. In addition, due to the complex environment, imperfect CSI is considered for all channels, i.e., $g_a = \tilde{g}_a + e_a$ and $g_\alpha = \tilde{g}_\alpha + e_\alpha$, where $\tilde{g}_a$ and $\tilde{g}_\alpha$ are the channel coefficients estimated by using the minimum mean square errors (MMSEs) for g_a and g_α, respectively, and $e_a, e_\alpha \sim \mathcal{CN}(0, \Omega_e)$, with Ω_e being the correctness of the channel estimation and $\mathcal{CN}(0, \Omega_e)$ being a scalar complex Gaussian distribution with zero mean and variance Ω_e [30].

B. Communication protocol

The basic idea of CR-NOMA is that the GBS sends a signal with transmit power P_P to the PR on an orthogonal frequency band in the primary network. In the secondary network, the ST may sense the frequency band from the GBS in order to transmit signals to D_p and D_q with the help of the multihop URs by applying the NOMA principle. The TS transmission protocol shown in Fig. 2 is used in [9] for communication in each time block T. Specifically, there is one phase for EH, followed by $(N+1)$ phases for signal transmission from the ST to the IDs, as follows:

- In the EH phase, to improve the energy consumption performance, the URs harvest energy from the PB. The energy harvested by the URs is formulated as

$$\mathcal{E}_{U_n} = \sum_{p=1}^{P} \delta_{U_n} \tau T \mathcal{P}_B \frac{g_{BU_n}}{\overline{L}_{BU_n}}, \quad (6)$$

where δ_{R_v} is the energy conversion efficiency of R_v; τ is the EH time, $0 < \tau < 1$; and $\mathcal{P}_B$

is the transmit power of the PB. Furthermore, the expected amount of energy harvested by the relays can be calculated by averaging over the power fading coefficients, as follows [27]:

$$\mathcal{E}_{U_n} = \sum_{p=1}^{P} \delta_{U_n} \tau T \mathcal{P}_B \frac{\Omega_{BU_n}}{\bar{L}_{BU_n}}. \tag{7}$$

- In the first communication phase, the ST transmits the superimposed signal x_S to D_χ, where $\chi \in \{p, q\}$, $x_S = \sqrt{\mu_p} x_p + \sqrt{\mu_q} x_q$, $\mu_p + \mu_q = 1$, and $\mu_p < \mu_q$. Therefore, the received signal at the first UR can be written as

$$y_{U_1} = \sqrt{\frac{P_S g_{SU_1}}{\bar{L}^{\theta}_{SU_1}}} \left(\sqrt{\mu_p} x_p + \sqrt{\mu_q} x_q \right) + n_{U_1}, \tag{8}$$

where $\mathcal{P}_S$ is the transmit power of the ST and $n_{U_1} \sim \mathcal{CN}(0, N_0)$. Applying the NOMA scheme, U_1 first decodes the q-th ID's information x_q by treating x_p as noise. U_1 then obtains x_p from the superimposed signal by using SIC [11]. Here, we consider imperfect SIC at the URs and IDs because of residual interference due to potential deployment problems (e.g., error propagation and complexity scaling). These unwanted errors in decoding are the main reason for the degradation in performance. Thus, the NOMA network will be affected by residual interference through the signal errors occurring because of imperfect SIC. Specifically, the interference term arising due to imperfect SIC at the URs and IDs is $I_S \sim \mathcal{CN}(0, \xi_S N_0)$ [5]. Therefore, the received signal-to-interference-plus-noise ratios (SINRs) at the first UR for decoding x_p and x_q are formulated as

$$\gamma^{(p)}_{U_1} = \frac{\mu_p P_S \tilde{g}_{SU_1}}{\bar{L}_{SU_1} \left(P_S \Omega_e + I_S + N_0 \right)}, \tag{9}$$

$$\gamma^{(q)}_{U_1} = \frac{\mu_q P_S \tilde{g}_{SU_1}}{\bar{L}_{SU_1} \left(\frac{\mu_p P_S \tilde{g}_{SU_1}}{\bar{L}_{SU_1}} + P_S \Omega_e + N_0 \right)}. \tag{10}$$

Meanwhile, the GBS broadcasts the signal x_P to the PR using the OMA principle. The ST interferes with the PR in the orthogonal frequency band due to its broadcast nature. Thus, the received signal at the PR in the first phase can be written as

$$y^{(1)}_P = \sqrt{\frac{P_P g_{G_v P}}{d^{\theta}_{G_v P}}} x_P + \sqrt{\frac{P_S g_{SP}}{d^{\theta}_{SP}}} x_S + n^{(1)}_P, \tag{11}$$

where $\mathcal{P}_P$ is the transmit power of the GBS and $n^{(1)}_P \sim \mathcal{CN}(0, N_0)$. Accordingly, the received SINR at the PR is formulated as

$$\gamma^{(1)}_P = \frac{P_P \tilde{g}_{G_v P}}{d^{\theta}_{G_v P} \left[\frac{P_S \tilde{g}_{SP}}{d^{\theta}_{SP}} + \left(P_S + P_P \right) \Omega_e + N_0 \right]}. \tag{12}$$

- In the second communication phase, the first UR uses the DF technique to decode the signal from the ST and forward it to the second UR. Thus, the received signal at the second UR can be written as

$$y_{U_2} = \sqrt{\frac{P_{U_1} g_{U_1 U_2}}{\bar{L}^{\theta}_{U_1 U_2}}} \left(\sqrt{\mu^{(1)}_p} x_p + \sqrt{\mu^{(1)}_q} x_q \right) + n_{U_2}, \tag{13}$$

where $n_{U_2} \sim \mathcal{CN}(0, N_0)$. Similar to the first communication phase, the received SINRs at the second UR for decoding x_p and x_q are formulated as

$$\gamma^{(p)}_{U_2} = \frac{\mu^{(1)}_p P_{U_1} \tilde{g}_{U_1 U_2}}{\bar{L}_{U_1 U_2} \left(P_{U_1} \Omega_e + I_S + N_0 \right)}, \tag{14}$$

$$\gamma^{(q)}_{U_2} = \frac{\mu^{(1)}_q P_{U_1} \tilde{g}_{U_1 U_2}}{\bar{L}_{U_1 U_2} \left(\frac{\mu^{(1)}_p P_{U_1} \tilde{g}_{U_1 U_2}}{\bar{L}_{U_1 U_2}} + P_{U_1} \Omega_e + N_0 \right)}. \tag{15}$$

Furthermore, due to the short distance from the first UR to the PR, interference from the UR affects the received signal at the PR, as follows:

$$y^{(2)}_P = \sqrt{\frac{P_P g_{G_v P}}{d^{\theta}_{G_v P}}} x_P + \sqrt{\frac{P_{U_1} g_{U_1 P}}{d^{\theta}_{U_1 P}}} x_S + n^{(2)}_P, \tag{16}$$

where $n^{(2)}_P \sim \mathcal{CN}(0, N_0)$. Thus, the received SINR at the PR in the second phase is formulated as

$$\gamma^{(2)}_P = \frac{P_P \tilde{g}_{G_v P}}{d^{\theta}_{G_v P} \left[\frac{P_{U_1} \tilde{g}_{U_1 P}}{\bar{L}_{U_1 P}} + \left(P_{U_1} + P_P \right) \Omega_e + N_0 \right]}. \tag{17}$$

- Similarly, in the n-th communication phase ($2 < n < N$), the $(n-1)$-th UR decodes and forwards the signal from the $(n-2)$-th UR to the n-th UR. Thus, the received signal at the n-th UR becomes

$$y_{U_n} = \sqrt{\frac{P_{U_{n-1}} g_{U_{n-1}U_n}}{\bar{L}^{\theta}_{U_{n-1}U_n}}} \times \left(\sqrt{\mu_p^{(n-1)}} x_p + \sqrt{\mu_q^{(n-1)}} x_q \right) + n_{U_n}, \tag{18}$$

where $n_{U_n} \sim \mathcal{CN}(0, N_0)$. Then, the received SINRs at the n-th UR for decoding x_p and x_q are

$$\gamma_{U_n}^{(p)} = \frac{\mu_p^{(n)} P_{U_{n-1}} \tilde{g}_{U_{n-1}U_n}}{\bar{L}_{U_{n-1}U_n} \left(P_{U_{n-1}} \Omega_e + I_S + N_0 \right)}, \tag{19}$$

$$\gamma_{U_n}^{(q)} = \frac{\mu_q^{(n)} P_{U_{n-1}} \tilde{g}_{U_{n-1}U_n}}{\bar{L}_{U_{n-1}U_n} \left(\begin{array}{c} \frac{\mu_p^{(n)} P_{U_{n-1}} \tilde{g}_{U_{n-1}U_n}}{\bar{L}_{U_{n-1}U_n}} \\ + P_{U_{n-1}} \Omega_e + N_0 \end{array} \right)}. \tag{20}$$

For the primary network, the received signal at the PR in the n-th phase is written as

$$y_P^{(n)} = \sqrt{\frac{P_P g_{G_v P}}{d^{\theta}_{G_v P}}} x_P + n_P^{(n)}, \tag{21}$$

where $n_P^{(n)} \sim \mathcal{CN}(0, N_0)$. The received SINR at the PR in the n-th phase is

$$\gamma_P^{(n)} = \frac{P_P \tilde{g}_{G_v P}}{d^{\theta}_{G_v P} \left(P_P \Omega_e + N_0 \right)}. \tag{22}$$

- In the N-th and $(N+1)$-th communication phases, the N-th UR and the IDs are affected by interference from the GBS because of the broadcast nature of the communication. Thus, the received signals at the N-th UR, D_p, and D_q respectively become

$$y_{U_N} = \sqrt{\frac{P_{U_{N-1}} g_{U_{N-1}U_N}}{\bar{L}_{U_{N-1}U_N}}} x_S + \sqrt{\frac{P_P g_{G_v U_N}}{d^{\theta}_{G_v U_N}}} x_P + n_{U_N}, \tag{23}$$

$$y_{D_p} = \sqrt{\frac{P_{U_N} g_{U_N D_p}}{\bar{L}_{U_N D_p}}} x_S + \sqrt{\frac{P_P g_{G_v D_p}}{d^{\theta}_{G_v D_p}}} x_P + n_{D_p}, \tag{24}$$

$$y_{D_q} = \sqrt{\frac{P_{U_N} g_{U_N D_q}}{\bar{L}_{U_N D_q}}} x_S + \sqrt{\frac{P_P g_{G_v D_q}}{d^{\theta}_{G_v D_q}}} x_P + n_{D_q}, \tag{25}$$

where $n_{U_N}, n_{D_p}, n_{D_q} \sim \mathcal{CN}(0, N_0)$. Accordingly, the SINRs at U_N, D_p, and D_q for decoding the p-th and q-th signals are

$$\gamma_{U_N}^{(p)} = \frac{\mu_p^{(N-1)} P_{U_{N-1}} \tilde{g}_{U_{N-1}U_N}}{\bar{L}_{U_{N-1}U_N} \left[\begin{array}{c} \frac{P_P \tilde{g}_{G_v U_N}}{\bar{L}_{G_v U_N}} + I_S + N_0 \\ + \left(P_P + P_{U_{N-1}} \right) \Omega_e \end{array} \right]}, \tag{26}$$

$$\gamma_{U_N}^{(q)} = \frac{\mu_q^{(N-1)} P_{U_{N-1}} \tilde{g}_{U_{N-1}U_N}}{\bar{L}_{U_{N-1}U_N} \left[\begin{array}{c} \frac{\mu_p^{(N-1)} P_{U_{N-1}} \tilde{g}_{U_{N-1}U_N}}{\bar{L}_{U_{N-1}U_N}} \\ + \frac{P_P \tilde{g}_{G_v U_N}}{\bar{L}_{G_v U_N}} + N_0 \\ + \left(P_P + P_{U_{N-1}} \right) \Omega_e \end{array} \right]}, \tag{27}$$

$$\gamma_{D_p}^{(p)} = \frac{\mu_p^{(N)} P_{U_N} \tilde{g}_{U_N D_p}}{\bar{L}_{U_N D_p} \left[\begin{array}{c} \frac{P_P \tilde{g}_{G_v D_p}}{d^{\theta}_{G_v D_p}} + I_S + N_0 \\ + \left(P_P + P_{U_N} \right) \Omega_e \end{array} \right]}, \tag{28}$$

$$\gamma_{D_q}^{(q)} = \frac{\mu_q^{(N)} P_{U_N} \tilde{g}_{U_N D_q}}{\bar{L}_{U_N D_q} \left[\begin{array}{c} \frac{\mu_p^{(N)} P_{U_N} \tilde{g}_{U_N D_q}}{\bar{L}_{U_N D_q}} + \frac{P_P \tilde{g}_{G_v D_q}}{d^{\theta}_{G_v D_q}} \\ + \left(P_P + P_{U_N} \right) \Omega_e + N_0 \end{array} \right]}. \tag{29}$$

Similar to the n-th phase, the received signals at the PR in the N-th and $(N+1)$-th phases are not affected by interference from the GBS. Accordingly, the received SINRs at the PR in the N-th and $(N+1)$-th phases are as $\gamma_P^{(N)} = \gamma_P^{(N+1)} = \gamma_P^{(n)}$. To improve the system performance, the GBS chooses its transmit antenna such that the SINRs at the PR are the best in each communication phase, i.e.,

$$v^* = \arg \max_{v \in \{1, \ldots, V\}} \gamma_P^{(n)}. \tag{30}$$

Furthermore, there exists an EAV near the IDs that is attempting to eavesdrop on the confidential signals under interference from the GBS. The received signal at the EAV is

$$y_E = \sqrt{\frac{P_{U_N} g_{U_N E}}{\bar{L}_{U_N E}}} x_S + \sqrt{\frac{P_P g_{G_v E}}{d^{\theta}_{G_v E}}} x_P + n_E, \tag{31}$$

where $n_E \sim \mathcal{CN}(0, N_0)$. Similar to a legitimate user, the EAV decodes x_q by treating x_p as noise and decodes x_p by means of imperfect SIC with residual interference $I_E \sim \mathcal{CN}(0, \xi_E N_0)$. Therefore, the SINRs at the EAV for eavesdropping on the p-th and q-th signals are

$$\gamma_E^{(p)} = \frac{\mu_p^{(N)} P_{U_N} \tilde{g}_{U_N E}}{\bar{L}_{U_N E} \left[\begin{array}{l} \frac{P_P \tilde{g}_{G_v E}}{d_{G_v E}^{\theta}} + (P_P + P_{U_N}) \Omega_e \\ + I_E + N_0 \end{array} \right]}, \tag{32}$$

$$\gamma_E^{(q)} = \frac{\mu_q^{(N)} P_{U_N} \tilde{g}_{U_N E}}{\bar{L}_{U_N E} \left[\begin{array}{l} \frac{\mu_p^{(N)} P_{U_N} \tilde{g}_{U_N E}}{\bar{L}_{U_N E}} + \frac{P_P \tilde{g}_{G_v E}}{d_{G_v E}^{\theta}} \\ + (P_P + P_{U_N}) \Omega_e + N_0 \end{array} \right]}. \tag{33}$$

According to the definition of the DF technique, with the note that $\gamma_U^{(\chi)} = \min_{n \in \{1,\ldots,N\}} \gamma_{U_n}^{(\chi)}$, the end-to-end SINRs for decoding the signals at the χ-th ID and the EAV are as follows [34]:

$$\gamma_{E2E,D_\chi}^{(\chi)} = \min\left\{\gamma_U^{(\chi)}, \gamma_{D_\chi}^{(\chi)}\right\}. \tag{34}$$

$$\gamma_{E2E,E}^{(\chi)} = \min\left\{\gamma_U^{(\chi)}, \gamma_E^{(\chi)}\right\}, \tag{35}$$

III. Performance Analysis and Problem Formulation

In this section, the system performance and secrecy performance of the CR-NOMA system are analyzed. Then, a problem formulation is defined in which the ST and the URs need to control their power allocations to ensure that the communication from the GBS to the PR is not degraded while maximizing the throughput of the secondary network.

First, the outage probability of the PR in all phases is defined as the probability of the channel capacity being smaller than a certain outage threshold R_P for the primary network, i.e.,

$$\mathcal{O}_P^{(n)} = \Pr\left\{C_P^{(n)} < R_P\right\}, \tag{36}$$

where $n \in \{1, \ldots, N+1\}$ and $C_P^{(n)}$ is the channel capacity of the GBS–PR link in the n-th phase with system bandwidth W, as follows:

$$C_P^{(n)} = \frac{W}{N+1} \log\left(1 + \gamma_P^{(n)}\right). \tag{37}$$

Lemma 1. *With the note that $n \in \{3, \ldots, N+1\}$ and $\partial_P = 2^{\frac{(N+1)R_P}{\mathrm{W}}} - 1$, the outage probabilities of the primary network in the first phase, second phase, and n-th phase are*

$$\mathcal{O}_P^{(1)} = \prod_{v=1}^{V} \left\{ \begin{array}{l} 1 - \exp\left[-\frac{\partial_P d_{G_{v^*P}}^{\theta}[(\rho_S+\rho_P)\Omega_e+1]}{\rho_P \Omega_{G_{v^*P}}}\right] \\ \times \frac{d_{SP}^{\theta} \rho_P \Omega_{G_{v^*P}}}{\partial_P d_{G_{v^*P}}^{\theta} \rho_S \Omega_{SP} + d_{SP}^{\theta} \rho_P \Omega_{G_{v^*P}}} \end{array} \right\}, \tag{38}$$

$$\mathcal{O}_P^{(2)} = \prod_{v=1}^{V} \left\{ \begin{array}{l} 1 - \frac{\exp\left\{-\frac{\partial_P d_{G_{v^*P}}^{\theta}\left[\left(\rho_{U_1}+\rho_P\right)\Omega_e+1\right]}{\rho_P \Omega_{G_{v^*P}}}\right\}}{\Omega_{SP}\Gamma\left(m_{U_1P}\right)} \\ \times \left(\frac{m_{U_1P}}{\Omega_{U_1P}}\right)^{m_{U_1P}} (m_{U_1P}-1)! \\ \left(\frac{\partial_P d_{G_{v^*P}}^{\theta} \rho_{U_1}}{\rho_P \Omega_{G_{v^*P}} \bar{L}_{U_1P}^{\theta}} + \frac{m_{U_1P}}{\Omega_{U_1P}}\right)^{-m_{U_1P}} \end{array} \right\}, \tag{39}$$

$$\mathcal{O}_P^{(n)} = \prod_{v=1}^{V} \left\{ 1 - \exp\left[-\frac{\partial_P d_{G_{v^*P}}^{\theta}\left(\rho_P \Omega_e + 1\right)}{\rho_P \Omega_{G_{v^*P}}}\right] \right\}, \tag{40}$$

Proof: See Appendix A.

Second, similar to Lemma 1, the outage probabilities of the secondary network for the p-th and q-th IDs are defined as the probabilities that their channel capacities are below a certain outage threshold for the secondary network, i.e.,

$$\mathcal{O}_S^{(\chi)} = \Pr\left\{C_S^{(\chi)} < R_S\right\}, \tag{41}$$

where R_S is the outage threshold at the IDs and $C_S^{(\chi)}$ is the channel capacity of the ST–D_χ link as

$$C_S^{(\chi)} = \frac{W}{N+1} \log\left(1 + \gamma_{E2E,D_\chi}^{(\chi)}\right). \tag{42}$$

Lemma 2. *The outage probability of the secondary network at the χ-th ID is*

$$\mathcal{O}_S^{(\chi)} = 1 - \mathbb{P}_1^{(\chi)} \times \mathbb{P}_2^{(\chi)} \times \mathbb{P}_3^{(\chi)} \times \mathbb{P}_4^{(\chi)}, \tag{43}$$

where $n \in \{2, \cdots, N-1\}$ and $\mathbb{P}_1^{(p)}$, $\mathbb{P}_2^{(p)}$, $\mathbb{P}_1^{(q)}$, $\mathbb{P}_2^{(q)}$, $\mathbb{P}_3^{(p)}$, $\mathbb{P}_4^{(p)}$, $\mathbb{P}_3^{(q)}$, and $\mathbb{P}_4^{(q)}$ are defined as follows:

$$\mathbb{P}_1^{(p)} = \sum_{j=0}^{m_{SU_1}-1} \frac{\left(\Delta_1^{(p)}\right)^j}{j!} \exp\left(-\Delta_1^{(p)}\right), \tag{44}$$

$$\mathbb{P}_2^{(p)} = \sum_{j=0}^{m_{U_{n-1}U_n}-1} \frac{\left(\Delta_2^{(p)}\right)^j}{j!} \exp\left(-\Delta_2^{(p)}\right), \tag{45}$$

$$\mathbb{P}_1^{(q)} = \sum_{j=0}^{m_{SU_1}-1} \left(\Delta_1^{(q)}\right)^j \frac{1}{j!} \exp\left(-\Delta_1^{(q)}\right), \tag{46}$$

$$\mathbb{P}_2^{(q)} = \sum_{j=0}^{m_{U_{n-1}U_n}-1} \left(\Delta_2^{(q)}\right)^j \frac{1}{j!} \exp\left(-\Delta_2^{(q)}\right), \tag{47}$$

$$\mathbb{P}_3^{(p)} = \exp\left(-\Delta_3^{(p)}\right) \left(\frac{m_{G_{v^*}U_N}}{\Omega_{G_{v^*}U_N}}\right)^{m_{G_{v^*}U_N}} \times \sum_{j=0}^{m_{U_{N-1}U_N}-1} \frac{1}{j!} \left(\frac{m_{U_{N-1}U_N}\partial_S \bar{L}_{U_{N-1}U_N}}{\Omega_{U_{N-1}U_N}\mu_p^{(N-1)}\rho_{U_{N-1}}}\right)^j \times \sum_{k=0}^{j} \frac{C_j^k \left[\left(\rho_P + \rho_{U_{N-1}}\right)\Omega_e + \xi_S + 1\right]^{j-k}}{\Gamma\left(m_{G_{v^*}U_N}\right)} \times \frac{\left(\frac{\rho_P}{\bar{L}_{G_{v^*}U_N}}\right)^k (k + m_{G_{v^*}U_N} - 1)!}{\left(\frac{m_{U_{N-1}U_N}\partial_S \bar{L}_{U_{N-1}U_N}\rho_P}{\Omega_{U_{N-1}U_N}\mu_p^{(N-1)}\rho_{U_{N-1}}\bar{L}_{G_{v^*}U_N}} + \frac{m_{G_{v^*}U_N}}{\Omega_{G_{v^*}U_N}}\right)^{k+m_{G_{v^*}U_N}}}, \tag{48}$$

$$\mathbb{P}_4^{(p)} = \sum_{j=0}^{m_{U_N D_p}-1} \frac{\exp\left(-\Delta_4^{(p)}\right)}{\Omega_{G_{v^*}D_p} j!} \left(\frac{m_{U_N D_p}\partial_S \bar{L}_{U_N D_p}}{\Omega_{U_N D_p}\mu_p^{(N)}\rho_{U_N}}\right)^j \times \sum_{k=0}^{j} C_j^k \left(\frac{\rho_P}{d_{G_{v^*}D_p}^{\theta}}\right)^k \left[\left(\rho_P + \rho_{U_N}\right)\Omega_e + \xi_S + 1\right]^{j-k} \times \frac{k!}{\left(\frac{m_{U_N D_p}\partial_S \bar{L}_{U_N D_p}\rho_P}{\Omega_{U_N D_p}\mu_p^{(N)}\rho_{U_N} d_{G_{v^*}D_p}^{\theta}} + \frac{1}{\Omega_{G_{v^*}D_p}}\right)^{k+1}}, \tag{49}$$

$$\mathbb{P}_3^{(q)} = \exp\left(-\Delta_3^{(q)}\left[\left(\rho_P + \rho_{U_{N-1}}\right)\Omega_e + 1\right]\right) \times \left(\frac{m_{G_{v^*}U_N}}{\Omega_{G_{v^*}U_N}}\right)^{m_{G_{v^*}U_N}} \sum_{j=0}^{m_{U_{N-1}U_N}-1} \frac{1}{j!}\left(\Delta_3^{(q)}\right)^j \times \sum_{k=0}^{j} \frac{C_j^k \left[\left(\rho_P + \rho_{U_{N-1}}\right)\Omega_e + 1\right]^{j-k}\left(\frac{\rho_P}{\bar{L}_{G_{v^*}U_N}}\right)^k}{\Gamma\left(m_{G_{v^*}U_N}\right)} \times \frac{(k + m_{G_{v^*}U_N} - 1)!}{\left(\frac{\Delta_3^{(q)}\rho_P}{\bar{L}_{G_{v^*}U_N}} + \frac{m_{G_{v^*}U_N}}{\Omega_{G_{v^*}U_N}}\right)^{k+m_{G_{v^*}U_N}}}, \tag{50}$$

$$\mathbb{P}_4^{(q)} = \frac{\exp\left(-\Delta_4^{(q)}\left[\left(\rho_P + \rho_{U_N}\right)\Omega_e + 1\right]\right)}{\Omega_{G_{v^*}D_p}} \times \sum_{j=0}^{m_{U_N D_p}-1} \frac{1}{j!}\left(\Delta_4^{(q)}\left[\left(\rho_P + \rho_{U_N}\right)\Omega_e + 1\right]\right)^j \times \sum_{k=0}^{j} C_j^k \left(\frac{\rho_P}{d_{G_{v^*}D_q}^{\theta}}\right)^k \left[\left(\rho_P + \rho_{U_N}\right)\Omega_e + 1\right]^{j-k} \times \frac{k!}{\left(\frac{\Delta_4^{(q)}\rho_P}{d_{G_{v^*}D_q}^{\theta}} + \frac{1}{\Omega_{G_{v^*}D_q}}\right)^{k+1}}, \tag{51}$$

with

$$\Delta_1^{(p)} = \frac{m_{SU_1}\partial_S \bar{L}_{SU_1}\left(\rho_S\Omega_e + \xi_S + 1\right)}{\Omega_{SU_1}\mu_p\rho_S}, \tag{52}$$

$$\Delta_2^{(p)} = \frac{m_{U_{n-1}U_n}\partial_S \bar{L}_{U_{n-1}U_n}\left(\rho_{U_{n-1}}\Omega_e + \xi_S + 1\right)}{\Omega_{U_{n-1}U_n}\mu_p^{(n)}\rho_{U_{n-1}}}, \tag{53}$$

$$\Delta_3^{(p)} = \frac{m_{U_{N-1}U_N}\partial_S \bar{L}_{U_{N-1}U_N}\left[\begin{array}{l}\left(\rho_P + \rho_{U_{N-1}}\right)\Omega_e \\ +\xi_S + 1\end{array}\right]}{\Omega_{U_{N-1}U_N}\mu_p^{(N-1)}\rho_{U_{N-1}}}, \tag{54}$$

$$\Delta_4^{(p)} = \frac{m_{U_N D_p}\partial_S \bar{L}_{U_N D_p}\left[\left(\rho_P + \rho_{U_N}\right)\Omega_e + \xi_S + 1\right]}{\Omega_{U_N D_p}\mu_p^{(N)}\rho_{U_N}}, \tag{55}$$

$$\Delta_1^{(q)} = \frac{m_{SU_1}\partial_S \bar{L}_{SU_1}\left(\rho_S\Omega_e + 1\right)}{\Omega_{SU_1}\left(\mu_q - \mu_p\partial_S\right)\rho_S}, \tag{56}$$

$$\Delta_2^{(q)} = \frac{m_{U_{n-1}U_n}\partial_S \bar{L}_{U_{n-1}U_n}\left(\rho_{U_{n-1}}\Omega_e + 1\right)}{\Omega_{U_{n-1}U_n}\left(\mu_q^{(n)} - \mu_p^{(n)}\partial_S\right)\rho_{U_{n-1}}}, \tag{57}$$

$$\Delta_3^{(q)} = \frac{m_{U_{N-1}U_N}\partial_S \bar{L}_{U_{N-1}U_N}}{\Omega_{U_{N-1}U_N}\left(\mu_q^{(N-1)} - \mu_p^{(N-1)}\partial_S\right)\rho_{U_{N-1}}}, \tag{58}$$

$$\Delta_4^{(q)} = \frac{m_{U_N D_q}\partial_S \bar{L}_{U_N D_q}}{\Omega_{U_N D_q}\left(\mu_q^{(N)} - \mu_p^{(N)}\partial_S\right)\rho_{U_N}}. \tag{59}$$

Proof: See Appendix B.

The outage probability is the primary criterion for assessing the dependability of multihop UAV CR-NOMA. However, the throughput of the secondary network is still needed to determine how well the system as a whole is functioning to ensure that transmissions are reliable. To evaluate the system performance, the throughput for the p-th and q-th IDs is calculated as $\mathcal{T}_S^{(\chi)} = \left(1 - \mathcal{O}_S^{(\chi)}\right) R_S$ [35].

Third, the EAV can monitor the confidential signals from the N-th UR due to their broadcast nature. It should be noted that the signal-to-noise ratio (SNR) at a legitimate user and that at the EAV are interdependent because the URs use the DF scheme. This complicates the effort to derive a tractable form for the secrecy outage probability in our considered problem and may even make such a derivation impossible. To overcome this issue, the information leakage probability is considered instead to evaluate the secrecy performance. This metric is defined as the probability that the channel

capacity from the ST to the EAV is higher than a certain leakage threshold R_E, as follows:

$$\mathcal{L}_S^{(\chi)} = \Pr\left\{C_E^{(\chi)} > R_E\right\}, \tag{60}$$

where $C_E^{(\chi)}$ is the channel capacity of the ST–E link for decoding the χ-th signal and is expressed as

$$C_E^{(\chi)} = \frac{W}{N+1}\log\left(1+\gamma_{E2E,E}^{(\chi)}\right). \tag{61}$$

Lemma 3. *The leakage probability of the secondary network at the EAV for monitoring the signal x_χ is*

$$\mathcal{L}_S^{(\chi)} = \mathbb{P}_{1,E}^{(\chi)} \times \mathbb{P}_{2,E}^{(\chi)} \times \mathbb{P}_{3,E}^{(\chi)} \times \mathbb{P}_{4,E}^{(\chi)}, \tag{62}$$

where $n \in \{2, \cdots, N-1\}$ and $\mathbb{P}_{1,E}^{(p)}$, $\mathbb{P}_{2,E}^{(p)}$, $\mathbb{P}_{3,E}^{(p)}$, $\mathbb{P}_{4,E}^{(p)}$, $\mathbb{P}_{1,E}^{(q)}$, $\mathbb{P}_{2,E}^{(q)}$, $\mathbb{P}_{3,E}^{(q)}$, and $\mathbb{P}_{4,E}^{(q)}$ are defined as follows:

$$\mathbb{P}_{1,E}^{(p)} = \sum_{j=0}^{m_{SU_1}-1} \frac{\left(\Delta_{1,E}^{(p)}\right)^j}{j!}\exp\left(-\Delta_{1,E}^{(p)}\right), \tag{63}$$

$$\mathbb{P}_{2,E}^{(p)} = \sum_{j=0}^{m_{U_{n-1}U_n}-1} \frac{\left(\Delta_{2,E}^{(p)}\right)^j}{j!}\exp\left(-\Delta_{2,E}^{(p)}\right), \tag{64}$$

$$\begin{aligned}\mathbb{P}_{3,E}^{(p)} =& \exp\left(-\Delta_{3,E}^{(p)}\right)\left(\frac{m_{G_{v^*}U_N}}{\Omega_{G_{v^*}U_N}}\right)^{m_{G_{v^*}U_N}} \\ &\times \sum_{j=0}^{m_{U_{N-1}U_N}-1} \frac{1}{j!}\left(\frac{m_{U_{N-1}U_N}\partial_E \bar{L}_{U_{N-1}U_N}}{\Omega_{U_{N-1}U_N}\mu_p^{(N-1)}\rho_{U_{N-1}}}\right)^j \\ &\times \sum_{k=0}^{j} \frac{C_j^k\left[\left(\rho_P+\rho_{U_{N-1}}\right)\Omega_e+\xi_E+1\right]^{j-k}}{\Gamma\left(m_{G_{v^*}U_N}\right)} \\ &\times \frac{\left(\frac{\rho_P}{\bar{L}_{G_{v^*}U_N}}\right)^k (k+m_{G_{v^*}U_N}-1)!}{\left(\frac{m_{U_{N-1}U_N}\partial_E \bar{L}_{U_{N-1}U_N}\rho_P}{\Omega_{U_{N-1}U_N}\mu_p^{(N-1)}\rho_{U_{N-1}}\bar{L}_{G_{v^*}U_N}} + \frac{m_{G_{v^*}U_N}}{\Omega_{G_{v^*}U_N}}\right)^{k+m_{G_{v^*}U_N}}},\end{aligned} \tag{65}$$

$$\begin{aligned}\mathbb{P}_{4,E}^{(p)} =& \sum_{j=0}^{m_{U_N E}-1} \frac{\exp\left(-\Delta_{4,E}^{(p)}\right)}{\Omega_{G_{v^*}E}j!}\left(\frac{m_{U_N E}\partial_E \bar{L}_{U_N E}}{\Omega_{U_N E}\mu_p^{(N)}\rho_{U_N}}\right)^j \\ &\times \sum_{k=0}^{j} C_j^k\left(\frac{\rho_P}{d_{G_{v^*}E}^{\theta}}\right)^k\left[\left(\rho_P+\rho_{U_N}\right)\Omega_e+\xi_E+1\right]^{j-k} \\ &\times \frac{k!}{\left(\frac{m_{U_N E}\partial_E \bar{L}_{U_N E}\rho_P}{\Omega_{U_N E}\mu_p^{(N)}\rho_{U_N}d_{G_{v^*}E}^{\theta}} + \frac{1}{\Omega_{G_{v^*}E}}\right)^{k+1}},\end{aligned} \tag{66}$$

$$\mathbb{P}_{1,E}^{(q)} = \sum_{j=0}^{m_{SU_1}-1}\left(\Delta_{1,E}^{(q)}\right)^j\frac{1}{j!}\exp\left(-\Delta_{1,E}^{(q)}\right), \tag{67}$$

$$\mathbb{P}_{2,E}^{(q)} = \sum_{j=0}^{m_{U_{n-1}U_n}-1}\left(\Delta_{2,E}^{(q)}\right)^j\frac{1}{j!}\exp\left(-\Delta_{2,E}^{(q)}\right), \tag{68}$$

$$\begin{aligned}\mathbb{P}_{3,E}^{(q)} =& \exp\left(-\Delta_{3,E}^{(q)}\left[\left(\rho_P+\rho_{U_{N-1}}\right)\Omega_e+1\right]\right) \\ &\times \left(\frac{m_{G_{v^*}U_N}}{\Omega_{G_{v^*}U_N}}\right)^{m_{G_{v^*}U_N}} \sum_{j=0}^{m_{U_{N-1}U_N}-1}\frac{1}{j!}\left(\Delta_{3,E}^{(q)}\right)^j \\ &\times \sum_{k=0}^{j}\frac{C_j^k\left[\left(\rho_P+\rho_{U_{N-1}}\right)\Omega_e+1\right]^{j-k}\left(\frac{\rho_P}{\bar{L}_{G_{v^*}U_N}}\right)^k}{\Gamma\left(m_{G_{v^*}U_N}\right)} \\ &\times \frac{(k+m_{G_{v^*}U_N}-1)!}{\left(\frac{\Delta_{3,E}^{(q)}\rho_P}{\bar{L}_{G_{v^*}U_N}} + \frac{m_{G_{v^*}U_N}}{\Omega_{G_{v^*}U_N}}\right)^{k+m_{G_{v^*}U_N}}},\end{aligned} \tag{69}$$

$$\begin{aligned}\mathbb{P}_{4,E}^{(q)} =& \frac{\exp\left(-\Delta_{4,E}^{(q)}\left[\left(\rho_P+\rho_{U_N}\right)\Omega_e+1\right]\right)}{\Omega_{G_{v^*}E}} \\ &\times \sum_{j=0}^{m_{U_N E}-1}\frac{1}{j!}\left(\Delta_{4,E}^{(q)}\left[\left(\rho_P+\rho_{U_N}\right)\Omega_e+1\right]\right)^j \\ &\times \sum_{k=0}^{j} C_j^k\left(\frac{\rho_P}{d_{G_{v^*}E}^{\theta}}\right)^k\left[\left(\rho_P+\rho_{U_N}\right)\Omega_e+1\right]^{j-k} \\ &\times \frac{k!}{\left(\frac{\Delta_{4,E}^{(q)}\rho_P}{d_{G_{v^*}E}^{\theta}} + \frac{1}{\Omega_{G_{v^*}E}}\right)^{k+1}},\end{aligned} \tag{70}$$

with

$$\Delta_{1,E}^{(p)} = \frac{m_{SU_1}\partial_E \bar{L}_{SU_1}\left(\rho_S\Omega_e+\xi_E+1\right)}{\Omega_{SU_1}\mu_p\rho_S}, \tag{71}$$

$$\Delta_{2,E}^{(p)} = \frac{m_{U_{n-1}U_n}\partial_E \bar{L}_{U_{n-1}U_n}\left(\rho_{U_{n-1}}\Omega_e+\xi_E+1\right)}{\Omega_{U_{n-1}U_n}\mu_p^{(n)}\rho_{U_{n-1}}}, \tag{72}$$

$$\Delta_{3,E}^{(p)} = \frac{m_{U_{N-1}U_N}\partial_E \bar{L}_{U_{N-1}U_N}\left[\begin{array}{l}\left(\rho_P+\rho_{U_{N-1}}\right)\Omega_e\\ +\xi_E+1\end{array}\right]}{\Omega_{U_{N-1}U_N}\mu_p^{(N-1)}\rho_{U_{N-1}}}, \tag{73}$$

$$\Delta_{4,E}^{(p)} = \frac{m_{U_N D_p}\partial_E \bar{L}_{U_N E}\left[\left(\rho_P+\rho_{U_N}\right)\Omega_e+\xi_E+1\right]}{\Omega_{U_N E}\mu_p^{(N)}\rho_{U_N}}, \tag{74}$$

$$\Delta_{1,E}^{(q)} = \frac{m_{SU_1}\partial_E \bar{L}_{SU_1}\left(\rho_S\Omega_e+1\right)}{\Omega_{SU_1}\left(\mu_q-\mu_p\partial_E\right)\rho_S}, \tag{75}$$

$$\Delta_{2,E}^{(q)} = \frac{m_{U_{n-1}U_n}\partial_E \bar{L}_{U_{n-1}U_n}\left(\rho_{U_{n-1}}\Omega_e+1\right)}{\Omega_{U_{n-1}U_n}\left(\mu_q^{(n)}-\mu_p^{(n)}\partial_E\right)\rho_{U_{n-1}}}, \tag{76}$$

$$\Delta_{3,E}^{(q)} = \frac{m_{U_{N-1}U_N}\partial_E \bar{L}_{U_{N-1}U_N}}{\Omega_{U_{N-1}U_N}\left(\mu_q^{(N-1)}-\mu_p^{(N-1)}\partial_E\right)\rho_{U_{N-1}}}, \tag{77}$$

$$\Delta_{4,E}^{(q)} = \frac{m_{U_N E}\partial_E \bar{L}_{U_N E}}{\Omega_{U_N E}\left(\mu_q^{(N)}-\mu_p^{(N)}\partial_S\right)\rho_{U_N}}. \tag{78}$$

Proof: See Appendix C.

Finally, the model proposed in this paper aims to guarantee that all legitimate IDs can receive and decode their required signals, in other words, that the p-th ID can decode x_p and the q-th ID can decode x_q. The core of the optimization problem is to determine not only the UR locations but also the number of URs and many other related parameters so as to ensure that the throughput of the IDs is maximized. Since the IDs are all placed within an area that can be covered by the last UR, all x_p and x_q can be decoded. In short, the objective is to maximize the throughput of the secondary network subject to the specified requirements on the outage probability of the primary network. In particular, we optimize the power allocation factors at the URs, i.e., μ_p and $\mu_p^{(n)}$; the transmit power levels of the PT, PB, and GBS; the number of URs; and the 3-D positions of the URs. Accordingly, the optimization problem can be formulated as follows:

$$\max_{\mathbf{d}} \left\{\mathcal{T}_S^{(p)}+\mathcal{T}_S^{(q)}\right\}, \tag{79}$$

$$\text{s.t. } P_S \le P_{\max}, \tag{80}$$

$$\mathcal{O}_P^{(n)} \le \varepsilon_P, \tag{81}$$

$$\mathcal{L}_E^{(p)}, \mathcal{L}_E^{(q)} \le \varepsilon_E, \tag{82}$$

$$\mu_p+\mu_q=1, \tag{83}$$

$$\mu_p^{(n)}+\mu_q^{(n)}=1, \tag{84}$$

where $n \in \{1,\ldots,N\}$ and $\mathbf{d}$ is a set of optimized parameters including μ_p, $\mu_p^{(n)}$, N, P_B, P_S, P_P, and the tuples $(x_n, y_n, h_n)|_{n=1,..,N}$. $P_{\max}$ is the maximum transmit power of the ST. Note that $\mathbf{d}$ does not include μ_q and $\mu_q^{(n)}$ because for a given μ_p and $\mu_p^{(n)}$, these two parameters are known via the relations in (83) and (84). The details of how $\mathbf{d}$ is constructed are given in (85). Meanwhile, (81) and (82) guarantee that the communication from the GBS to the PR is not degraded and that the EAV cannot decode the confidential signals from the last UR, respectively.

IV. Machine Learning Design

In this subsection, we present the detailed construction of the input to our proposed hybrid method and the structure of its algorithm, which exploits both the quick greedy convergence of PSO and the efficient exploration ability of a GA.

First, we observe that the problem given in (79)–(84) is a complex nonlinear optimization problem with multiple local maxima. It is characterized by a high-dimensional continuous search space (P_B, P_S, P_P, number of URs, positions of the URs, power allocation factors μ_p and μ_q) subject to a set of constraints. Therefore, we combine PSO not with a classic GA but rather with the continuous GA (CGA), an improved variant of a GA that can handle a large number of continuous variables. In CGA, we construct a chromosome as a vector of real values. Specifically, the k-th chromosome in the t-th generation is

$$\mathbf{d}_k^{(t)} = [\mu_p, \mu_p^{(n)}, N, [x_n, y_n, h_n]_{N\times 3}, P_B, P_S, P_P], \tag{85}$$

and the input to the algorithm consists of the objective function defined in (79) and the control parameters of the algorithm itself.

It can be seen from (85) that the total number of dimensions of the candidates can vary because the number of URs, N, is considered a parameter to be optimized, and the dimensions of the matrix $[x_n, y_n, h_n]_{N\times 3}$ vary with N. This implies that if a new solution candidate uses more URs than the previous solution candidate, then the locations of these additional URs must be added into that candidate's chromosome and optimized. To make heuristic search methods applicable, we modify the candidate chromosome $\mathbf{d}_k^{(t)}$ by fixing the N dimen-

Algorithm 1 Proposed Hybrid CGA-PSO Algorithm

Initialize
λ, r_c, r_m, T, and $t = 0$;
    \\T is the maximum number of generations/iterations
Generate the initial population $\mathbf{d}_k^{(t)}$, $k = 1, \ldots, \lambda$;
for ($t = 1$ to T) **do**
    for ($k = 1$ to λ) **do**
        Evaluate the fitness of chromosome k: $\mathbf{f_k^{(t)}} = Fitness\left(\mathbf{d}_k^{(t)}\right)$ as in (90);
    end for
    Reproduce chromosomes based on their fitnesses;
    Apply crossover by combining two parents and the
        memorized current best individual with r_c, as
        in (87) and (88);
    Apply mutation to offspring with r_m;
    \\New population is formed
end for
Output the best chromosomes;

sion of the matrix $[x_n, y_n, h_n]_{N\times 3}$ to its upper-bound value $N = N_{\max}$; thus, (85) becomes

$$\mathbf{d}_k^{(t)} = [\mu_p, \mu_p^{(n)}, N, [x_n, y_n, h_n]_{N_{\max}\times 3}, P_B, P_S, P_P], \tag{86}$$

where $N_{\max}$ is the maximum number of URs. Therefore, if $N < N_{\max}$ for a certain candidate solution, then only the 1st to N-th rows of the matrix $[x_n, y_n, h_n]_{N_{\max}\times 3}$ matter. The proposed algorithm begins with random chromosomes in the initial population $\mathbf{d}_k^{(0)}$. Then, each chromosome in the population is evaluated by means of the objective function, and in the selection step, good chromosomes are chosen for reproduction so as to maintain the population size λ. In the crossover step, most chromosomes are recombined in pairs with a crossover rate r_c to create new pairs of chromosomes, called offspring. Specifically, when the proposed hybrid CGA-PSO algorithm chooses a pair of individuals $\mathbf{d}_i^{(t)}$ and $\mathbf{d}_j^{(t)}$, it produces two new candidates $\mathbf{d}_i^{(t+1)}$ and $\mathbf{d}_j^{(t+1)}$ as follows:

$$\mathbf{d}_i^{(t+1)} = u_1\mathbf{d}_i^{(t)} + u_2\mathbf{d}_j^{(t)} + u_3\mathbf{d}_{best}^{(t)}, \tag{87}$$
$$\mathbf{d}_j^{(t+1)} = u_2\mathbf{d}_i^{(t)} + u_1\mathbf{d}_j^{(t)} + u_3\mathbf{d}_{best}^{(t)}, \tag{88}$$

where the u_i are uniform random values satisfying $u_i > 0$ and $\sum_{i=1}^{3} u_i = 1$. This is the key feature of our method. For the creation of offspring, the proposed crossover mechanism combines not merely two parents, as in other GA variants, but rather three parents, one of which is the current memorized best individual over all previous generations. This allows both a local search (exploring the search area around each parent) and a greedy uphill search (using the best candidate for guidance). This mechanism is actually a hybrid of CGA and PSO, in which new offspring individuals tend to move toward the current memorized best individual. Note that the new crossover procedure incurs only a few additional multiplications to introduce the influence of $\mathbf{d}_{best}^{(t)}$ and thus does not significantly increase the run time compared to CGA while leveraging both the advantage of CGA in escaping from local maxima and the advantage of PSO in achieving rapid convergence.

The final step of each generation t is mutation, in which chromosomes are chosen at a low mutation rate r_m and a random value is added to each entry of the chosen chromosomes. These random values are drawn from a Gaussian distribution whose mean and deviation are 0 and 1/20 of the upper-bound entry length, respectively. The mutation step encourages genetic diversity within the population, which is necessary because chromosomes usually become increasingly homogeneous after a sufficiently large number of generations. Thus, the chromosomes evolve through multiple generations following a loop consisting of the selection, crossover, and mutation steps. When this generation loop terminates, the current memorized best chromosome is returned as the optimization result:

$$\mathbf{d}^* = [\mu_p^*, \mu_p^{(n)*}, N^*, [x_n, y_n, h_n]^*_{N_{\max}\times 3}, P_B^*, P_S^*, P_P^*]. \tag{89}$$

We also simplify the constrained optimization problem to a standard form by modifying the objective function to add penalties if any constraints

are violated. Specifically, the fitness value for an individual solution candidate is calculated as

$$\begin{aligned} Fitness\left(\mathbf{d}_k\right) &= \left\{\mathcal{T}_S^{(p)} + \mathcal{T}_S^{(q)}\right\} \\ &- \mathrm{w}_1\mathbf{max}(0, P_S - P_{max}) - \mathrm{w}_2\mathbf{max}(0, \mathcal{O}_P^{(n)} - \varepsilon_P) \\ &- \mathrm{w}_3\mathbf{max}(0, \mathcal{L}_E^{(p)} - \varepsilon_E) - \mathrm{w}_4\mathbf{max}(0, \mathcal{L}_E^{(q)} - \varepsilon_E), \end{aligned} \tag{90}$$

where $\mathrm{w}_i > 0$ to ensure that the penalties are valid.

To explain the results reported later, convergence and complexity analyses are also presented in this section. First, we analyze the convergence model of the proposed GA. Due to the procedure of roulette selection, the probability $p_{t+1}\left(\mathbf{d}_i\right)$ of choosing an individual $\mathbf{d}_i$ for reproduction when producing generation $t+1$ is proportional to its fitness f_i in generation t. Thus, the probability distribution is

$$p_{t+1}\left(d_i\right) = \frac{f_i}{\sum_j f_j}. \tag{91}$$

Because individual $\mathbf{d}_i$ is not unique but can be duplicated in the population, the probability of f_i in generation $t+1$ depends on the number of duplicates of $\mathbf{d}_i$, $N_{i,t}$, in generation t. This probability becomes

$$p_{t+1}\left(f_i\right) = N_{i,t}\frac{f_i}{\sum_j f_j} = \frac{N_{i,t}}{N}\frac{f_i}{\frac{\sum_j f_{j,t}}{N}} = \frac{f_i}{\overline{f_{i,t}}}p_t\left(f_i\right). \tag{92}$$

In any generation t, $\overline{f_{i,t}}$ has a specific value; thus, without loss of generality, (92) can be rewritten as

$$p_{t+1}\left(f\right) = a_{t+1} f\, p_t\left(f\right), \tag{93}$$

where a_{t+1} is the normalization factor necessary to make $p_{t+1}\left(f\right)$ a PDF, or $\int_{-\infty}^{+\infty} p_{t+1}\left(f\right) df = 1$.

From (93), it is also derived that

$$p_{t+1}\left(f\right) \propto f\, p_t\left(f\right) \propto f^2 p_{t-1}\left(f\right) \propto ... \propto f^t p_0\left(f\right). \tag{94}$$

The distribution of f is increasingly driven by f^t as the population is affected by the selection procedure over generations, causing the probability of individuals with low f to approach zero and that of individuals with high f to increase exponentially. We can see the convergence trend by assuming that f is uniformly distributed in generation $t = 0$ and that the maximum fitness function value is M (see Fig. 3). Then, for generation t, from $p_t\left(f\right) \propto f^t\, p_0\left(f\right)$, we have $p_t\left(f\right) = a_t f^t$. Using the constraint $\int_0^M a_t f^t df = 1$, we obtain $a_t = \frac{t+1}{M^{t+1}}$.

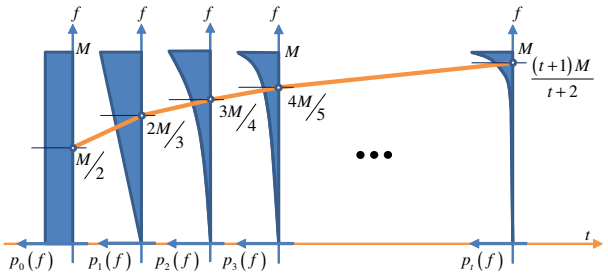

Fig. 3: Convergence characteristics under the effect of the selection mechanism.

Given a_t as found in this way, the average fitness value in generation t becomes

$$\begin{aligned} \overline{f_t} &= \int_0^M f\, a_t f^t df = \frac{t+1}{M^{t+1}}\int_0^M f^{t+1} df \\ &= \frac{t+1}{t+2}M = 1 - \frac{M}{t+2}. \end{aligned} \tag{95}$$

Specifically, $\overline{f_0} = \frac{M}{2}$, $\overline{f_1} = \frac{2M}{3}$, $\overline{f_2} = \frac{3M}{4}$, and so on. This value asymptotically approaches the maximum fitness value M at a speed of $\frac{M}{t+2}$ for generation t, as illustrated in Fig. 3. This convergence trend of the average fitness explains the observed behavior of the mean curves in Fig. 11.

It can be seen that the convergence tendency of a GA is basically determined by the selection stage. In the crossover and mutation stages, new individuals are created to perform a local search and increase the opportunity to find candidates that are better than the current best candidate. In other words, by virtue of crossover and mutation, M should not remain fixed over the generations but should instead be updated to higher values throughout the execution of the algorithm. According to the above analysis, the convergence tendency will always be maintained with each new M. As a result, the mean fitness value does not always smoothly increase with successive generations t but instead exhibits spikes due to the emergence of new M_t values by virtue of crossover and mutation, as illustrated in Fig. 4. Note that the convergence curve of the mean fitness also fluctuates because of the random nature of the search driven by mutation even when mutation does not cause M to be updated. Our hybrid method has a better chance of finding better M values than other methods because the crossover mechanism combines three parents instead of only two. This means that our method performs its local search not

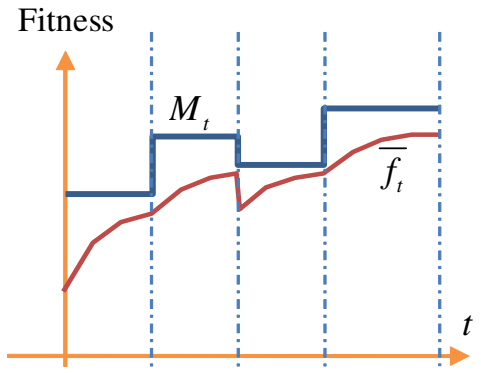

Fig. 4: Convergence of $\overline{f_t}$ with updated M_t values over successive generations t.

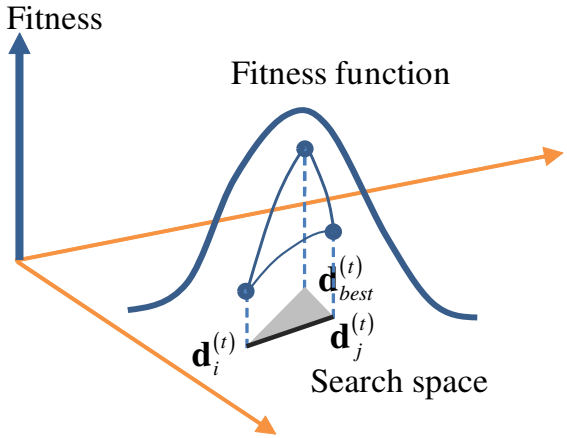

Fig. 5: Crossover analysis of the proposed hybrid CGA-PSO method.

only along the line connecting $\mathbf{d}_i$ and $\mathbf{d}_i$ but also within the triangle formed by $\mathbf{d}_i$, $\mathbf{d}_i$, and $\mathbf{d}_{best}$ (see the gray triangle depicted in Fig. 5). In addition, since $f(\mathbf{d}_{best}) \geq f(\mathbf{d}_i)$ and $f(\mathbf{d}_{best}) \geq f(\mathbf{d}_j)$, our local search has a more uphill greedy nature, and thus, the new offspring individuals have a better chance of achieving high fitness values, causing the mean $\overline{f_t}$ to converge faster.

Second, as seen in Algorithm 1, the computational complexity lies mainly in the **for** loops. The first **for** loop is for producing generation t (line 4), while the others are for processing each individual in the population in each generation. Since our objective function is based on a feed-forward closed form (no feedback), each calculation of the fitness function can be considered to be of the same complexity, $O(1)$. Therefore, the complexity of computing the fitness of the whole population is $O(\lambda)$. One **for** loop is also needed to address crossover and mutation, with a complexity of $O(p_c\lambda + p_r\lambda)$. However, the selection of good chromosomes for reproduction is based on the roulette wheel selection method (line 9). Thus, a complexity of $O(\lambda)$ is needed to form the "wheel" array, while for each newly produced individual, the complexity of determining the section on the "wheel" to each random "dart" belongs is $O(\log_2(\lambda))$. As a result, the overall complexity of the hybrid algorithm is

$$O\left\{T\left[\begin{array}{l} O(\lambda) + O(p_c\lambda + p_r\lambda) \\ +O(\lambda) + O(\lambda \log_2 \lambda) \end{array}\right]\right\} \simeq O(T\lambda \ln \lambda), \tag{96}$$

where it should be noted that $O(\lambda \ln \lambda) > O(\lambda)$.

V. Numerical Results

In this section, numerical results are presented to analyze the outage probability of the considered CR-NOMA system and the convergence of Algorithm 1. Without loss of generality, we investigate the considered system with the following system parameters [30], [32]. We set the fading parameters to $m_a = m_\alpha = 2$, the system bandwidth to $W = 100$ MHz, the number of URs to $N = \{3, 4, 5\}$, the thresholds of the IDs and PR for successfully decoding their signals to $R_S = 10$ and $R_P = 100$, and the leakage threshold to $R_E = 10$. Furthermore, we investigate URs operating in an urban environment with the parameters $\varphi = 9.6177$, $\psi = 0.1581$, $\omega_{\text{LoS}} = 1$, and $\omega_{\text{NLoS}} = 20$ [9].

In Fig. 6, we plot the impact of the transmit power at the ST and the channel estimation error on the outage probability at the PR with $N = 4$. It is observed that as P_S increases, the outage probability at the PR in the first phase also increases. This is because the high transmit power of the ST leads to more interference at the PR. In the remaining phases, i.e., the second phase to the fourth phase, the outage probability at the PR is constant because the ST is not affected by the remaining URs. Furthermore, as Ω_e increases, the outage probability of the primary network increases because knowledge of the channel information decreases as the channel estimation error increases. Similarly, Fig. 7 depicts

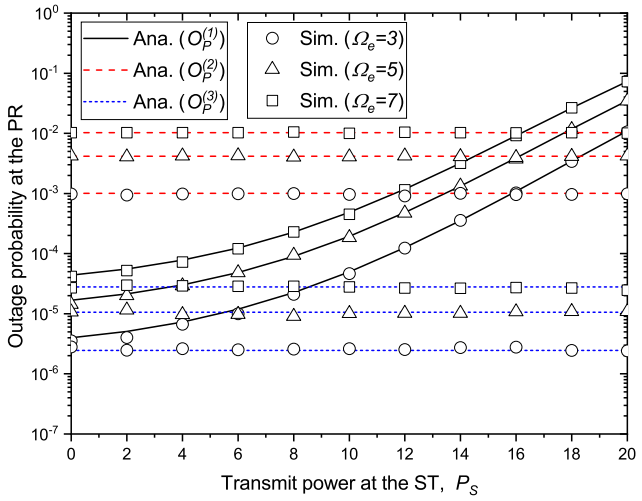

Fig. 6: Impact of the transmit power at the ST and the channel estimation error on the outage probability of the primary network.

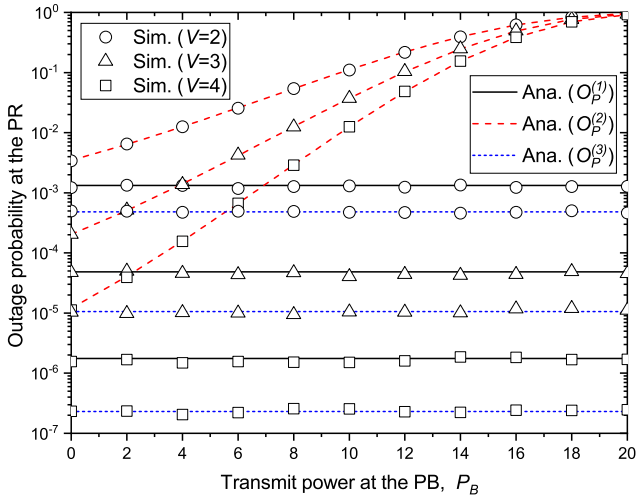

Fig. 7: Impact of the transmit power at the PB and the number of antennas of the GBS on the outage probability of the primary network.

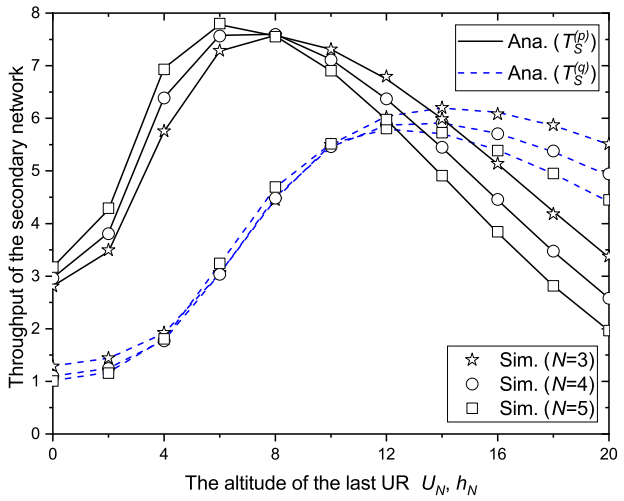

Fig. 8: Impact of the altitude of the last UR and the outage threshold γ_S on the throughput of the secondary network.

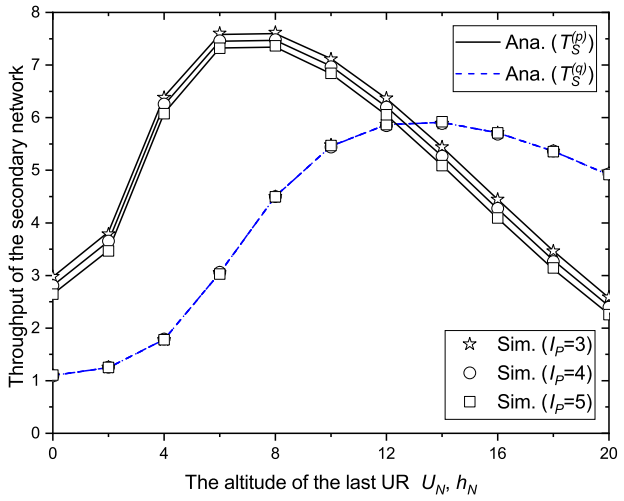

Fig. 9: Impact of the altitude of the last UR and different values of I_P on the throughput of the secondary network.

the effects of the transmit power at the PB and the number of antennas of the GBS on $\mathcal{O}_P^{(n)}$ in the second phase. We can see that the outage probability at the PR improves when $\mathcal{P}_\mathcal{B}$ is low. This is because a smaller $\mathcal{P}_\mathcal{B}$ leads to a smaller transmit power of U_1. As a result, the effect on the PR caused by interference from U_1 is not significant when the transmit power at the PB is low. In the first, third and fourth phases, $\mathcal{P}_\mathcal{B}$ remains the same as $\mathcal{P}_\mathcal{B}$ increases because the URs do not interfere with the PR. Furthermore, the outage probability at the PR decreases as the number of antennas at the GBS increases. This is because a larger number of antennas leads to a higher diversity gain.

Fig. 8 illustrates the throughput of the secondary network for various values of the last UR's altitude and the number of URs, N. We can see that $\mathcal{T}_S^{(p)}$ and $\mathcal{T}_S^{(q)}$ reach an optimal point when h_N takes a specific value, for the following reasons. When the N-th UR is flying at a high altitude, the probability of LoS conditions is high; however, the path loss also becomes large when the altitude

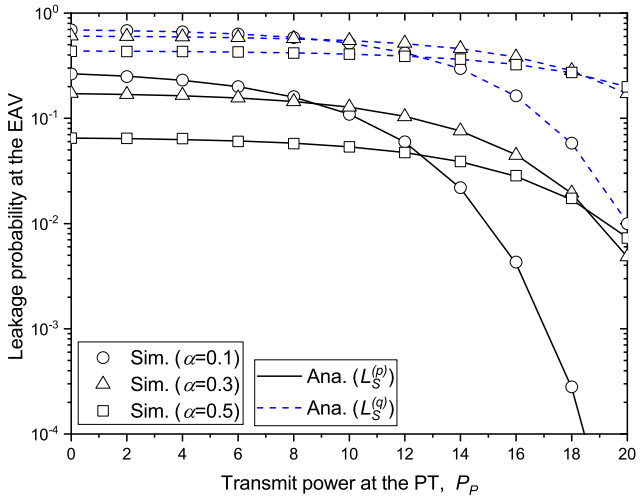

Fig. 10: Impact of the transmit power at the PT and the EH time α on the leakage probability at the EAV.

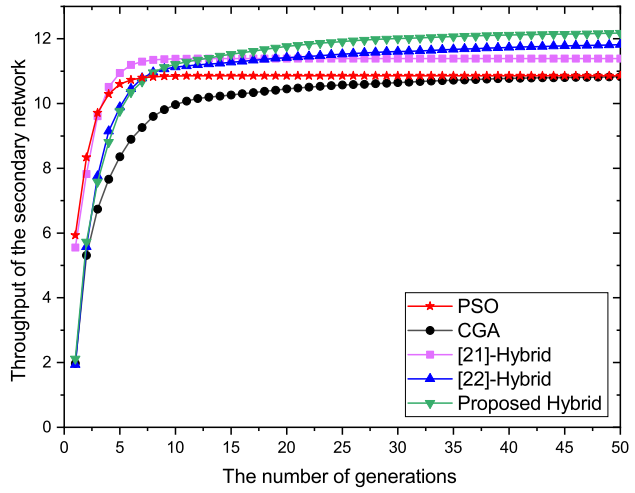

Fig. 11: Convergence behaviors of various heuristic methods, including PSO, CGA, the hybrid methods of [21] [22], and our proposed hybrid CGA-PSO method, over successive generations.

is very high. Furthermore, the throughput of the secondary network is better with a large N than with a small N when h_N is low, and vice versa. This is because when the altitude of the last UR is low, the probability of NLoS conditions is high. Thus, when more URs are used, the system performance of the secondary network will improve. In contrast, when h_N is high, the probability of NLoS conditions is decreased, leading to better throughput with a lower N than with a higher N. Similarly, Fig. 9 shows the throughput of the secondary network for various values of the last UR's altitude and I_P. It can be observed that as I_P increases, the throughput of the p-th ID decreases. This is because the residual interference signal imposes more noise on the p-th ID and the URs for the decoding of x_p. Meanwhile, $\mathcal{T}_S^{(q)}$ is always the same because the imperfect SIC does not affect the decoding process of the q-th ID.

Fig. 10 depicts the impact of the EH time and the transmit power at the PT on the leakage probability at the EAV. For both the p-th and q-th IDs, we find that the leakage probabilities decrease as the transmit power at the PT increases. This is because as P_P increases, the EAV receives more interference. Furthermore, a smaller α, i.e., a shorter EH time, leads to lower transmit power at the URs. Thus, the leakage probability is more strongly affected by the transmit power at the PT. This means that as P_P increases, the leakage probability at the EAV decreases more significantly. In contrast, both $\mathcal{L}_E^{(p)}$ and $\mathcal{L}_E^{(q)}$ decrease less as P_P increases. Furthermore, as τ approaches 0, the outage probability of the secondary network approaches 1 according to (43) since the transmit power of the URs reaches 0, indicating that the communication fails. In contrast, as the EH time increases, the outage probability decreases. This means that the system performance of the secondary network is improved. It should also be noted that a high τ leads to a high leakage probability at the EAV, causing the secrecy performance to decrease. This is the trade-off between system performance and secrecy performance. Accordingly, we have proposed the hybrid CGA-PSO algorithm to find the system parameters, including τ, that maximize the throughput while guaranteeing the secrecy performance.

Next, the results of optimization are presented in Fig. 11 and Table I for comparison with other population-based heuristic algorithms, i.e., CGA, PSO, and the hybrid methods of [21] and [22]. This figure depicts the convergence behavior over 50 generations ($T = 50$) for all methods, including our proposed hybrid CGA-PSO method described in Algorithm 1. Notably, the convergence speeds and final objective values are different. CGA converges slowly, and no good final objective value is found within 50 generations. In contrast, PSO converges quickly; the objective value stops improving after the 10th generation. Note that each curve in Fig. 11

is the average curve of the whole population over the generations. The results indicate that PSO achieves the greediest search but has a high probability of becoming trapped in a local maximum. Regarding the hybrid methods, although the method of [21] achieves quicker convergence than that of [22], its ability to escape local maxima is not as much improved as that of [22]. In comparison, it can be seen that our proposed hybrid CGA-PSO method has the best ability to escape local maxima so as to reach the global maximum, while its convergence behavior over successive generations is as good as that of [22].

TABLE I: Run-time comparison

	Number of generations to achieve 95% convergence	Run time (s) for 50 generations	Final average objective value $\mathcal{T}_S^{(p)} + \mathcal{T}_S^{(q)}$
CGA	16.20	0.7813	10.8270
PSO	4.10	0.4193	10.8589
Hybrid [21]	4.72	0.8472	11.3918
Hybrid [22]	16.18	1.3034	11.8190
Proposed	15.90	0.8015	12.1744

It should be noted that the convergence speed here is measured based only on the number of generations. However, the actual run time also matters because different methods involve different computation procedures and thus have different computational costs. Table I shows that CGA takes 16.2 generations to reach convergence, and the actual run time to complete 50 generations is 0.7813 seconds. In contrast, PSO needs fewer than 5 generations to converge and takes only 0.4193 seconds to complete 50 generations. This means that PSO is strictly superior to CGA on our problem, with a shorter actual run time and a higher objective value. For the hybrid methods of [21] and [22], global convergence is achieved with higher probability than for CGA or PSO. However, the trade-off for this is longer actual run times of 0.8472 and 1.3034 seconds, respectively. When the proposed hybrid CGA-PSO algorithm is compared with the remaining four, it is obviously superior to the hybrid method of [21] in terms of both the final objective value and the actual run time. In fact, the proposed hybrid algorithm yields the best objective value while needing only a 2.6% longer run time than CGA. This implies that the proposed hybrid method does face a trade-off when attempting to improve the fitness value of the result, but its trade-off is better than those of the hybrid methods of both [21] and [22]. Thus, our method clearly outperforms the previous hybrid methods and is a good choice for any similar complicated constrained optimization problems with high-dimensional search spaces.

VI. Conclusions

This paper has studied the system performance of a CR-NOMA system assisted by multiple URs. A corresponding communication protocol with an EH phase and multiple communication phases has been proposed. Accordingly, expressions for the outage probability at the PR, the throughput of the secondary network, and the leakage probability at the EAV have been obtained to analyze the system performance and secrecy performance. Based on this analysis, a new hybrid CGA-PSO algorithm has been proposed for determining the optimal power allocation and configuration of the URs to achieve the best throughput under constraints on the performance and security of the primary network. This hybrid model combines the strengths of CGA and PSO in terms of the ability to escape from local optima and the speed of convergence, respectively. Finally, numerical results show that the proposed hybrid CGA-PSO algorithm can satisfy the desired requirements on the system and secrecy performances. In our future work, we will investigate multiple-input multiple-output (MIMO) IoT systems with a nonlinear EH UAV model.

Appendix A
Proof of **Lemma 1**

By substituting (37) and (30) into (36), the outage probability of the primary network in the first phase can be obtained:

$$\mathcal{O}_P^{(1)} = \Pr\left\{\max_{v\in\{1,\ldots,V\}}\left\{\gamma_P^{(1)}\right\} < 2^{\frac{(N+1)\gamma_P}{\mathrm{W}}} - 1\right\}$$
$$= \prod_{v=1}^{V} \underbrace{\Pr\left\{\gamma_P^{(1)} < 2^{\frac{(N+1)\gamma_P}{\mathrm{W}}} - 1\right\}}_{\mathbb{P}_P^{(1)}}. \quad (97)$$

Next, by substituting (12) into the probability $\mathbb{P}_P^{(1)}$, we obtain

$$\mathbb{P}_P^{(1)} = \Pr\left\{ \frac{\rho_P \tilde{g}_{G_{v^*}P}}{d_{G_{v^*}P}^{\theta} \left[\begin{array}{l} \frac{\rho_S \tilde{g}_{SP}}{d_{SP}^{\theta}} + 1 \\ + (\rho_S + \rho_P)\,\Omega_e \end{array} \right]} < \partial_P \right\}, \tag{98}$$

where $\rho_P = P_P/N_0$ and $\rho_S = P_S/N_0$. Based on the definition of conditional probability and by using the CDFs and PDFs of the channel gains g_{DP} and g_{SP}, $\mathbb{P}_P^{(1)}$ can be formulated as

$$\mathbb{P}_P^{(1)} = \int_0^{\infty} \frac{1}{\Omega_{SP}} \exp\left(-\frac{x}{\Omega_{SP}}\right) \times \left\{ 1 - \exp\left[-\frac{\partial_P d_{G_{v^*}P}^{\theta} \left[\begin{array}{l} \frac{\rho_S x}{d_{SP}^{\theta}} + 1 \\ + (\rho_S + \rho_P)\,\Omega_e \end{array} \right]}{\rho_P \Omega_{G_{v^*}P}} \right] \right\} dx \tag{99}$$

With some mathematical manipulations, (99) can be rewritten as

$$\mathbb{P}_P^{(1)} = 1 - \frac{\exp\left[-\frac{\partial_P d_{G_{v^*}P}^{\theta} [(\rho_S + \rho_P)\Omega_e + 1]}{\rho_P \Omega_{G_{v^*}P}} \right]}{\Omega_{SP}} \times \int_0^{\infty} \left\{ \exp\left[-\left(\frac{\partial_P d_{G_{v^*}P}^{\theta} \rho_S}{d_{SP}^{\theta} \rho_P \Omega_{G_{v^*}P}} + \frac{1}{\Omega_{SP}} \right) x \right] \right\} dx. \tag{100}$$

Then, by applying the exponential function in [36, (3.310.11)], the closed-form expression for the outage probability of the PR in the first phase is obtained as given in (38). Similarly, the outage probability of the primary network in the second communication phase, $\mathcal{O}_P^{(2)}$, is given as (101), where $\rho_{U_1} = P_{U_1}/N_0$. By applying the exponential function with more complicated arguments presented in [36, (3.326.2)], $\mathcal{O}_P^{(2)}$ is obtained as given in (39). Similar to the approach for obtaining $\mathcal{O}_P^{(1)}$ and $\mathcal{O}_P^{(2)}$, $\mathcal{O}_P^{(3)}$ is obtained as presented in (40). This completes the proof.

Appendix B
Proof of Lemma 2

By substituting (34) and (42) into (41) and remark that $\partial_S = 2^{\frac{(N+1)\gamma_S}{\mathrm{W}}} - 1$, we obtain

$$\mathcal{O}_S^{(p)} = \Pr\left\{ \min\left\{ \gamma_{U_1}^{(p)}, \gamma_{U_n}^{(p)}, \gamma_{U_N}^{(p)}, \gamma_{D_p}^{(p)} \right\} < \partial_S \right\}. \tag{102}$$

From (102), we can formulate the outage probability of the secondary network for the p-th signal as

$$\mathcal{O}_S^{(p)} = 1 - \mathbb{P}_1^{(p)} \times \mathbb{P}_2^{(p)} \times \mathbb{P}_3^{(p)} \times \mathbb{P}_4^{(p)}, \tag{103}$$

where $\mathbb{P}_1^{(p)}$, $\mathbb{P}_2^{(p)}$, $\mathbb{P}_3^{(p)}$, and $\mathbb{P}_4^{(p)}$ are presented in (104), (105), (106), and (107), respectively.

By using some basic mathematical manipulations and the CDF of the channel gain, the probabilities $\mathbb{P}_1^{(p)}$ and $\mathbb{P}_2^{(p)}$ can be obtained as shown in (44) and (45). Meanwhile, the probabilities $\mathbb{P}_3^{(p)}$ and $\mathbb{P}_4^{(p)}$ are rewritten as presented in (108) and (109). Then, using the binomial formula [36, (1.111)] and combinations of exponential and rational functions [36, (3.351)], we can derive (50) and (51). Similarly, the outage probability of the secondary network for the q-th signal is obtained as given in (43). This completes the proof.

Appendix C
Proof of Lemma 3

By substituting (61) and (35) into (60), we obtain

$$\mathcal{L}_S^{(p)} = \Pr\left\{ \min\left\{ \gamma_{U_1}^{(p)}, \gamma_{U_n}^{(p)}, \gamma_{U_N}^{(p)}, \gamma_E^{(p)} \right\} > \partial_E \right\}, \tag{110}$$

where $\partial_E = 2^{\frac{(N+1)R_E}{\mathrm{W}}} - 1$. Similar to Appendix B, we can obtain the leakage probability as shown in (62) by exchanging (28) for (32) and (29) for (33). This completes the proof.

Acknowledgment

This work was supported by grants from Enthuse Company Limited, Kasetsart University, and Khon Kaen University, Thailand.

$$\mathcal{O}_P^{(2)} = \prod_{v=1}^{V} \left\{ 1 - \frac{\left(\frac{m_{U_1P}}{\Omega_{U_1P}}\right)^{m_{U_1P}} \exp\left[-\frac{\partial_P d^{\theta}_{G_{v^*P}}\left[\left(\rho_{U_1}+\rho_P\right)\Omega_e+1\right]}{\rho_P \Omega_{G_{v^*P}}}\right]}{\Gamma\left(m_{U_1P}\right)} \right.$$
$$\left. \times \int_0^{\infty} \exp\left[-\left(\frac{\partial_P d^{\theta}_{G_{v^*P}} \rho_{U_1}}{\rho_P \Omega_{G_{v^*P}} \bar{L}^{\theta}_{U_1P}} + \frac{m_{U_1P}}{\Omega_{U_1P}} \right) x \right] x^{m_{U_1P}-1} dx \right\}. \tag{101}$$

$$\mathbb{P}_1^{(p)} = 1 - \Pr\left\{ \tilde{g}_{SU_1} < \frac{\partial_S \bar{L}_{SU_1}\left(\rho_S \Omega_e + \xi_S + 1\right)}{\mu_p \rho_S} \right\}, \tag{104}$$

$$\mathbb{P}_2^{(p)} = 1 - \Pr\left\{ \tilde{g}_{U_{n-1}U_n} < \frac{\partial_S \bar{L}_{U_{n-1}U_n}\left(\rho_{U_{n-1}} \Omega_e + \xi_S + 1\right)}{\mu_p^{(n)} \rho_{U_{n-1}}} \right\}, \tag{105}$$

$$\mathbb{P}_3^{(p)} = 1 - \Pr\left\{ \tilde{g}_{U_{N-1}U_N} < \frac{\partial_S \bar{L}_{U_{N-1}U_N}\left[\frac{\rho_P \tilde{g}_{G_{v^*U_N}}}{\bar{L}_{G_{v^*U_N}}} + \left(\rho_P + \rho_{U_{N-1}}\right)\Omega_e + \xi_S + 1\right]}{\mu_p^{(N-1)} \rho_{U_{N-1}}} \right\}, \tag{106}$$

$$\mathbb{P}_4^{(p)} = 1 - \Pr\left\{ \tilde{g}_{U_N D_p} < \frac{\partial_S \bar{L}_{U_N D_p}\left[\frac{\rho_P \tilde{g}_{G_{v^*D_p}}}{d^{\theta}_{G_{v^*D_p}}} + \left(\rho_P + \rho_{U_N}\right)\Omega_e + \xi_S + 1\right]}{\mu_p^{(N)} \rho_{U_N}} \right\}. \tag{107}$$

$$\mathbb{P}_3^{(p)} = \left(\frac{m_{G_{v^*U_N}}}{\Omega_{G_{v^*U_N}}}\right)^{m_{G_{v^*U_N}}} \exp\left(-\frac{m_{U_{N-1}U_N} \partial_S \bar{L}_{U_{N-1}U_N}\left[\left(\rho_P + \rho_{U_{N-1}}\right)\Omega_e + \xi_S + 1\right]}{\Omega_{U_{N-1}U_N} \mu_p^{(N-1)} \rho_{U_{N-1}}} \right)$$
$$\times \sum_{j=0}^{m_{U_{N-1}U_N}-1} \frac{1}{j!} \left(\frac{m_{U_{N-1}U_N} \partial_S \bar{L}_{U_{N-1}U_N}}{\Omega_{U_{N-1}U_N} \mu_p^{(N-1)} \rho_{U_{N-1}}} \right)^j \int_0^{\infty} \left(\frac{\rho_P x}{\bar{L}_{G_{v^*U_N}}} + \left(\rho_P + \rho_{U_{N-1}}\right)\Omega_e + \xi_S + 1 \right)^j$$
$$\times \frac{x^{m_{G_{v^*U_N}}-1}}{\Gamma\left(m_{G_{v^*U_N}}\right)} \exp\left(-\left(\frac{m_{U_{N-1}U_N} \partial_S \bar{L}_{U_{N-1}U_N} \rho_P}{\Omega_{U_{N-1}U_N} \mu_p^{(N-1)} \rho_{U_{N-1}} \bar{L}_{G_{v^*U_N}}} + \frac{m_{G_{v^*U_N}}}{\Omega_{G_{v^*U_N}}} \right) x \right) dx, \tag{108}$$

$$\mathbb{P}_4^{(p)} = \exp\left(-\frac{m_{U_N D_p} \partial_S \bar{L}_{U_N D_p}\left[\left(\rho_P + \rho_{U_N}\right)\Omega_e + \xi_S + 1\right]}{\Omega_{U_N D_p} \mu_p^{(N)} \rho_{U_N}} \right) \sum_{j=0}^{m_{U_N D_p}-1} \frac{1}{\Omega_{G_{v^*D_p}} j!} \left(\frac{m_{U_N D_p} \partial_S \bar{L}_{U_N D_p}}{\Omega_{U_N D_p} \mu_p^{(N)} \rho_{U_N}} \right)^j$$
$$\times \int_0^{\infty} \left\{ \left[\frac{\rho_P x}{d^{\theta}_{G_{v^*D_p}}} + \left(\rho_P + \rho_{U_N}\right)\Omega_e + \xi_S + 1 \right]^j \exp\left(-\frac{m_{U_N D_p} \partial_S \bar{L}_{U_N D_p} \rho_P x}{\Omega_{U_N D_p} \mu_p^{(N)} \rho_{U_N} d^{\theta}_{G_{v^*D_p}}} - \frac{x}{\Omega_{G_{v^*D_p}}} \right) \right\} dx. \tag{109}$$

REFERENCES

[1] C. Huang, G. Chen, Y. Gong, and Z. Han, "Joint buffer-aided hybrid-duplex relay selection and power allocation for secure cognitive networks with double deep q-network," *IEEE Trans. on Cognitive Commun. and Networking*, vol. 7, no. 3, pp. 834–844, Mar. 2021.

[2] X. Deng, P. Guan, C. Hei, F. Li, J. Liu, and N. Xiong, "An intelligent resource allocation scheme in energy harvesting cognitive wireless sensor networks," *IEEE Trans. on Network Science and Engineering*, vol. 8, no. 2, pp. 1900–1912, May 2021.

[3] V. Aswathi and V. A. Babu, "Performance analysis of NOMA-based underlay cognitive radio networks with partial relay selection," *IEEE Trans. on Vehicular Tech.*, vol. 70, no. 5, pp. 4615–4630, Apr. 2021.

[4] V. N. Vo, C. So-In, D.-D. Tran, and H. Tran, "Optimal system performance in multihop energy harvesting WSNs using cooperative NOMA and friendly jammers," *IEEE Access*, vol. 7, pp. 125 494–125 510, Sep. 2019.

[5] D.-T. Do, A.-T. Le, and B. M. Lee, "NOMA in cooperative underlay cognitive radio networks under imperfect SIC," *IEEE Access*, vol. 8, pp. 86 180–86 195, May 2020.

[6] Z. Xiang, W. Yang, G. Pan, Y. Cai, and Y. Song, "Physical layer security in cognitive radio inspired NOMA network," *IEEE J. of Selected Topics in Signal Processing*, vol. 13, no. 3, pp. 700–714, Jul. 2019.

[7] Z. Wang, J. Guo, Z. Chen, Y. W. L. Yu, and H. Rao, "Robust secure UAV relay-assisted cognitive communications with resource allocation and cooperative jamming," *J. of Commun. and Networks*, vol. 24, no. 2, pp. 139–153, Apr. 2022.

[8] L. Sboui, H. Ghazzai, Z. Rezki, and M. Alouini, "On the throughput of cognitive radio MIMO systems assisted with UAV relays," in *proc Intern. Wireless Commun. and Mobile Computing Conf.*, 2017, pp. 939–944.

[9] B. Ji, Y. Li, S. Chen, C. Han, C. Li, and H. Wen, "Secrecy outage analysis of UAV assisted relay and antenna selection for cognitive network under nakagami-m channel," *IEEE Trans. on Cognitive Commun. and Networking*, vol. 7, pp. 1–11, Jan. 2020.

[10] D. Chi-Nguyen, P. N. Pathirana, M. Ding, and A. Seneviratne, "Secrecy performance of the UAV enabled cognitive relay network," in *proc Intern. Conf. on Commun. and Inform. Systems*, 2018, pp. 117–121.

[11] A. Bhowmick, S. Roy, and S. Kundu, "Throughput maximization of a UAV assisted CR network with NOMA-based communication and energy-harvesting," *IEEE Trans. on Vehicular Tech.*, vol. 71, no. 1, pp. 362–374, Jan. 2022.

[12] H. Li and X. Zhao, "Throughput maximization with energy harvesting in uav-assisted cognitive mobile relay networks," *IEEE Trans. on Cognitive Commun. and Networking*, vol. 7, no. 1, pp. 197–209, Mar. 2021.

[13] B. Ji, Y. Li, D. Cao, C. Li, S. Mumtaz, and D. Wang, "Secrecy performance analysis of UAV assisted relay transmission for cognitive network with energy harvesting," *IEEE Trans. on Veh. Tech.*, vol. 69, no. 7, pp. 7404–7415, Jul. 2020.

[14] Y. Zhou, F. Zhou, H. Zhou, D. W. K. Ng, and R. Q. Hu, "Robust trajectory and transmit power optimization for secure UAV-enabled cognitive radio networks," *IEEE Trans. on Commun.*, vol. 68, no. 7, pp. 4022–4034, Jul. 2020.

[15] H. M. A. Abdullah and A. V. S. Kumar, "HFSA-SORA: Hybrid firefly simulated annealing based spectrum opportunistic routing algorithm for cognitive radio Ad hoc networks (crahn)," in *proc. Intern. Conf. Intelligent Comput. and Control*, Jun. 2017, pp. 1–10.

[16] F. Okoli, J. Bert, S. Abdelaziz, N. Boussion, and D. Visvikis, "Optimizing the beam selection for noncoplanar VMAT by using simulated annealing approach," *IEEE Trans. Radiation Plasma Medical Sci.*, vol. 6, no. 5, pp. 609–618, May 2022.

[17] D. K. Luong, M. Ali, Y. F. Hu, J. P. Li, R. Asif, and K. Abdo, "Simulated annealing-based multilink selection algorithm in SDN-enabled avionic networks," *IEEE Access*, vol. 9, pp. 145 301–145 316, Oct. 2021.

[18] A. M. Yesaswini and K. Annapurna, "GA and PSO based spectrum allotment in cognitive radio networks," in *Intern. Conf. Inventive Computat. Techn.*, Feb. 2021, pp. 701–704.

[19] H. E. S. Hassan, A. E. D. S. Hafez, and A. A. Saied, "Optimum cognitive radio networks performance in AWGN using genetic algorithm," in *Intern. Telecommun. Conf.*, Jul. 2021, pp. 1–4.

[20] M. G. C. P and V. T, "Analysis and performance evaluation of pso for spectrum allocation in CRN," in *Intern. Conf. Innovative Practices Techno. and Management*, Apr. 2021, pp. 119–124.

[21] M. Yan, H. Yuan, and J. Xu, "Task allocation and route planning of multiple UAVs in a marine environment based on an improved particle swarm optimization algorithm," *EURASIP Journal on Advances in Signal Processing*, vol. 2021, no. 94, pp. 1–23, Oct. 2021.

[22] Z. Liu, J. Liu, F. Zhou, R. W. Liu, and N. Xiong, "A robust GA/PSO-hybrid algorithm in intelligent shipping route planning systems for maritime traffic networks," *Journal of Internet Technology*, vol. 19, no. 6, pp. 1635–1644, Nov. 2019.

[23] F. Javidrad and M. Nazari, "A new hybrid particle swarm and simulated annealing stochastic optimization method," *Applied Soft Computing*, vol. 60, pp. 634–654, Nov. 2017.

[24] K. Brezinski and K. Ferens, "Cognitive hybrid PSO/SA combinatorial optimization," in *proc. Intern. Conf. Cognitive Informatics & Cognitive Computing*, Jul. 2019, pp. 389–393.

[25] S. Anil, M. Pappa, and C. Ramesh, "Implementation of MIMO OFDM NOMA system using iterative algorithm," *IOP Conference Series: Materials Science and Engineering*, vol. 1166, no. 1, pp. 12–42, jul 2021.

[26] B. Ji, Y. Li, B. Zhou, C. Li, K. Song, and H. Wen, "Performance analysis of UAV relay assisted IoT communication network enhanced with energy harvesting," *IEEE Access*, vol. 7, pp. 38 738–38 747, Mar. 2019.

[27] H. Tran, T. X. Quach, H. Tran, and E. Uhlemann, "Optimal energy harvesting time and transmit power in cognitive radio network under joint constraints of primary users and eavesdroppers," in *Proc. Int. Symp. on Personal, Indoor and Mobile Radio Commun.*, Oct. 2017, pp. 1–8.

[28] X. Cao, X. Wang, and X. Lin, "Design and implementation of a centralized routing protocol for wireless sensor network," in *Proc. Int. Conf. Sensing Tech.*, Nov. 2016, pp. 1–6.

[29] T. H. Pham, X. J. Li, P. H. J. Chong, and Y. W. Leong, "Design and implementation of a centralized routing protocol for wireless sensor network," in *Proc. Int. Conf. Commun. Software and Net.*, Nov. 2010, p. 88–92.

[30] V. N. Q. Bao, T. Q. Duong, and C. Tellambura, "On the performance of cognitive underlay multihop networks with imperfect channel state information," *IEEE Trans. Commun.*, vol. 61, no. 12, pp. 4864–4873, Dec. 2013.

[31] Y. Li, R. Zhang, J. Zhang, S. Gao, and L. Yang, "Cooperative jamming for secure UAV communications with partial eavesdropper information," *IEEE Access*, vol. 7, pp. 94 593–94 603, Jul. 2019.

[32] Y. Chen, N. Zhao, and Z. D. M.-S. Alouini, "Multiple UAVs as relays: Multi-hop single link versus multiple dual-hop links," *IEEE Trans. Wireless Commun.*, vol. 17, no. 9, pp. 6348–6359, Aug. 2018.

[33] M. F. Sohail, C. Y. Leow, and S. Won, "Non-orthogonal

multiple access for unmanned aerial vehicle assisted communication," *IEEE Access*, vol. 6, pp. 22 716–22 727, Apr. 2018.

[34] H. Lei, Z. Dai, K. H. Park, W. Lei, G. Pan, and M. S. Alouini, "Secrecy outage analysis of mixed RF-FSO downlink SWIPT systems," *IEEE Trans. Commun.*, vol. 66, no. 12, pp. 6384–6395, 2018.

[35] D. Chen, W. Yang, J. HU, Y. CAI, and X. Tang, "Energy-efficient secure transmission design for the internet of things with an untrusted relay," *IEEE Access*, vol. 6, pp. 11 862–11 872, Feb. 2018.

[36] I. Gradshteyn and I. Ryzhik, *Table of Integrals, Series, and Products*, 8th ed., D. Zwillinger and V. Moll, Eds. Elsevier, 2014.